Lagrangian spin parameter and coherent structures from trajectories released in a high-resolution ocean model

by

Milena Veneziani[1]

Annalisa Griffa[1,2]

Zulema D. Garraffo[1]

Eric P. Chassignet[1]

[1]RSMAS/MPO, University of Miami, Miami, USA

[2]IOF/CNR, La Spezia, Italy

Corresponding author address:

Milena Veneziani
RSMAS/MPO 4600 Rickenbacker Cswy
Miami, FL 33149, USA
E-mail: cveneziani@rsmas.miami.edu
Tel.: +1 305 361-4654

Submitted to the

Journal of Marine Research

February 3, 2005

Abstract

A study of the mesoscale eddy field in presence of coherent vortices by means of Lagrangian trajectories released in a high-resolution ocean model is presented in this paper. The investigation confirms previous results drawn from real float data statistics (Veneziani et al., 2004), that the eddy field characteristics are due to the superposition of two distinct regimes associated with strong coherent vortices and with a typically more quiescent background eddy flow. The former gives rise to looping trajectories characterized by subdiffusivity properties due to the trapping effect of the vortices, while the latter produces non-looping floats characterized by simple diffusivity features. Moreover, the present work completes the study by Veneziani et al. (2004) in regard to the nature of the spin parameter Ω, which was used in the Lagrangian stochastic model that best described the observed eddy statistics.

The main results is that the spin obtained from the looping trajectories not only represents a good estimate of the relative vorticity of the vortex core in which the loopers are embedded, but it is also able to follow the vortex temporal evolution. The Lagrangian parameter Ω is then directly connected to the underlying Eulerian structure and could be used as a proxy for the relative vorticity field of coherent vortices.

1 Introduction

The mesoscale flow field is known to give a substantial contribution to the total energy content and transport of the ocean circulation. Although theoretical studies and high-resolution models, on the one side (e.g., Holland and Rhines, 1980; Alves and Colin de Verdiere, 1999; Marshall et al., 2002; Jayne and Marotzke, 2002), and observational efforts carried out mainly on regional and sub-basin scales, on the other (e.g., Bryden and Brady, 1989; Chereskin et al., 2000; Phillips and Rintoul, 2000; Roemmich and Gilson, 2001; Bower et al., 2002; Leach et al., 2002), have helped gain new insights into the role played by eddies in the large scale dynamical scenario, many aspects of the eddy dynamics and transport of momentum, mass, heat, and biochemical properties remain to be thoroughly investigated.

In the context of studying the mesoscale horizontal transport of passive tracers, Lagrangian data constitutes a natural and very useful framework because they are able to approximately follow the ocean currents at sub- and mesoscale scales. They are also potentially able to sample various temporal and spatial scales (depending on their specific characteristics), to provide broad horizontal coverage and information at depth. For these reasons, previous investigations by means of Lagrangian data have given insights into the characteristics of the large- and mesoscale flow, in terms of mean circulation and eddy kinetic energy content (e.g., Davis, 1991; Owens, 1991; Bograd et al., 1999; Shenoi et al., 1999; Fratantoni, 2001; Poulain, 2001), flow diffusivity and particle dispersion properties (e.g., Freeland et al., 1975; Riser and Rossby, 1983; Krauss and Boning, 1987; Figueroa and Olson, 1989; LaCasce, 2000), mixing capability (LaCasce and Bower, 2000), etc.

Lagrangian data also provide a direct way to test the validity of eddy transport parameterization methods, either by evaluating statistics and parameters to be adopted in eddy-diffusivity models (e.g., Bauer et al., 1998; Davis, 1998; Straneo et al., 2003), or by considering applications of Lagrangian Stochastic (LS) models (e.g., Falco et al., 2000; Bauer et al., 2002; Berloff et al., 2002). The LS models have been used in oceanography and physics of the atmosphere to represent the eddy contribution of particle dispersion in local and sub-basin scale studies (e.g., Thomson, 1986; Griffa, 1996; Berloff et al., 2002; Reynolds, 2002*a*). By increasing the complexity of the LS model it is possible to reproduce increasingly more complex statistical eddy properties (Berloff et al., 2002; Reynolds, 2002*b*, 2003).

Previous analyses of surface Lagrangian data (Krauss and Boning, 1987; Poulain and Niiler, 1989; Falco et al., 2000) suggest that, in regions not dominated by strong horizontally sheared currents or other coherent structures, one-dimensional, linear, LS models of the first-order are sufficient to describe the basic characteristics of the eddy field, such as Gaussian velocity probability distribution (pdf), exponentially decaying velocity autocovariance functions, and diffusive eddy field at times longer than the Lagrangian decorrelation time scale T_L [particle dispersion linearly increasing with time for $t \gg T_L$ as from Taylor's hypotheses (Taylor, 1921)].

On the other hand, investigations in dynamically more complex areas (Bauer et al., 1998, 2002; Berloff and McWilliams, 2002; Berloff et al., 2002) have revealed that such a simple model description does not apply when the eddy dynamics is dominated by the presence of coherent structures such as current jets, wave fields, and coherent vortices. These findings have been confirmed recently by Veneziani et al. (2004, hereafter VGRM) who have analyzed the historical data set of 700 m acoustically-tracked floats in the northwest Atlantic, focusing on the highly energetic and complex Gulf Stream recirculation area, in order to investigate possible LS models capable of describing the observed features. As already envisioned by Richardson (1993), VGRM show that the eddy transport results from a superposition of two different regimes, one associated with coherent vortices which are able to trap particles for long periods of time and give rise to looping trajectories, and one regime associated with a typically more quiescent background flow which produces non-looping floats. Such separation of turbulent regimes resembles the situation typically observed in quasi-geostrophic and two-dimensional turbulence dynamics (e.g., Elhmaidi et al., 1993; Bracco et al., 2000*b*; Pasquero et al., 2001), in which highly energetic coherent vortices form and affect not only particle dispersion at a local level through trapping mechanisms, but also the background eddy field by inducing anomalous diffusion and non-gaussianities in the velocity pdf due to their high energy content. Although the VGRM results at 700 m are reminiscent of this scenario, departures may be expected because of the more complex ocean dynamics, and because of the nature of the oceanic mesoscale vortices, which are not always isolated but interacting with other, equally energetic, coherent structures, and whose formation can be due to a variety of forcing mechanisms. Further investigations are needed, at the ocean surface and at different depth levels, to better assess relationships between oceanic and quasi-geostrophic turbulence dynamics.

VGRM show that the two regimes associated with looping and non-looping trajectories can be parameterized using a linear, first-order, two-dimensional, Lagrangian stochastic model with a “spin” parameter Ω. The spin is related to the angular velocity of the eddy velocity vector, and it couples the zonal and meridional velocity components of the eddy field (two-dimensionality property) reproducing the effects of coherent mesoscale vortices. The analysis is performed in selected quasi-homogeneous subregions, where the eddy field can be characterized by a specific set of parameter values. In particular, the spin is considered as a random parameter whose probability distribution is approximately bi-modal, with looping trajectories characterized by a finite value of Ω and non-looping floats associated to a zero value of spin. This simple bi-modal model is found to be effective in reproducing the main observed statistical properties of the eddy field.

It has to be noticed that the VGRM approach does not consider the non-local influence of the coherent vortices on the background eddy field. Previous works (Bracco et al., 2000*a*,*b*) indicate that the presence of vortices induces non-gaussianities in the background-flow pdfs, and that, at least in quasi-geostrophic turbulence (e.g., Pasquero et al., 2001), the background field cannot be fully described by a linear, first-order, autoregressive process because of the far-field influence of the energetic vortex structures. These effects have not been tested in VGRM because of the insufficient in-situ data sampling present in the geographically limited regions of investigation. Further studies are needed to address these points in oceanic applications.

Despite the positive VGRM results, some questions are left open. In particular, a detailed analysis of the spin parameter distribution in each of the considered subregions indicates that the bi-modality hypothesis may be oversimplifying. In some cases, different loopers seem to be characterized by different values of Ω, while in other cases single loopers show significant variations of spin during their time evolution. This leads to the question of whether the scattered values of Ω are indeed due to a more complex vortex population and to the change of vortex characteristics with time, or whether they are merely due to a sampling artifact resulting from the looper relative position with respect to the vortex edges. The issue also raises the more general question of what is the quantitative relationship between the properties of Lagrangian statistics and those of the underlying Eulerian field, in terms of regime separation and physical interpretation of the eddy parameters.

These points can be summarized into the following specific questions: what does the spin parameter Ω represent, besides describing the angular velocity of the Lagrangian velocity vector? Can the spin be interpreted as a quantity with a specific Eulerian meaning such as an estimate of relative vorticity for the vortex in which the particles are embedded? Is the occurrence of different values of Ω an effect of Lagrangian sampling of different areas of the vortex, or is it related to substantial variations of the vortex itself? Addressing these issues constitutes the main objective of the present work, allowing us to consolidate our previous results obtained from in-situ data, and also to provide a relatively simple tool to apply in both Lagrangian and Eulerian studies of mesoscale transport in presence of coherent vortices. In fact, if a robust relationship between the spin and the Eulerian vorticity is established, the simple computation of the Lagrangian Ω could give a direct assessment of the relative vorticity field in a complex flow, which is a more difficult task to achieve from Eulerian measurements.

These questions were not addressed in VGRM because of insufficient in-situ data sampling, on the one side, and because of the lack of available information on the underlying Eulerian field, on the other. Therefore, in this paper we consider results from a high-resolution numerical model, the Miami Isopycnic Coordinate Ocean Model (MICOM), where a large set of synthetic Lagrangian data has been released at 700 m depth. The large amount of simulated trajectories allows to overcome the problem of limited data coverage, while the availability of the modeled Eulerian fields permits to follow the history of the Eulerian structures together with the Lagrangian data interacting with them.

The adopted methodology consists in first identifying a region of interest in the modeled Gulf Stream recirculation area, and then characterizing the region in terms of Lagrangian eddy statistics and specific dynamical features. The method of investigation is similar to the one used by VGRM in that a regional study is carried out, and the region identification is based on quasi-homogeneous characteristics of eddy energy and dynamics. A more complete assessment of the region dynamical features is possible here with respect to VGRM, because of the availability of the MICOM predicted Eulerian flow field and ocean status. The paper is then dedicated to addressing the open questions outlined above by considering the contemporaneous evolution of the Eulerian and Lagrangian fields with their corresponding statistics, in the selected region of interest.

Specifically, the work is organized as follows. Section 2 presents the MICOM model and the synthetic Lagrangian data set. Section 3 describes the methodology, providing a brief background on the definition and estimate of the spin parameter from Lagrangian data and presenting the identification of the particular region of interest. Section 4 presents the results from the statistical analyses of the modeled trajectories in this region and the comparison with the in-situ results of VGRM. The questions concerning the physical meaning of the spin Ω and its relationship with the Eulerian vorticity in the vortex core are addressed in section 5. Finally, section 6 summarizes the main conclusions of the paper and briefly discusses future developments.

2 MICOM synthetic Lagrangian data

The Miami Isopycnic Coordinate Ocean Model [1] (MICOM) is a high-resolution primitive-equation model of the ocean circulation which has been well documented in the past (Bleck et al., 1992; Bleck and Chassignet, 1994). The particular configuration considered here covers the North and

[1]Updated information can be found online at http://oceanmodeling.rsmas.miami.edu/micom/.

Equatorial Atlantic Ocean from $28°$S to $70°$N, including the Caribbean Sea, the Gulf of Mexico, and the Mediterranean Sea. The bottom topography is derived from a digital terrain data set with $2.5'$ latitude-longitude resolution (ETOPO2.5). The external forcing consists of the ECMWF monthly climatological data obtained from the reanalysis of the 1979-1999 atmospheric data sets.

The horizontal model grid is defined on a Mercator projection and it has resolution of $1/12° \times 1/12° \cos(\phi)$ (where ϕ is latitude), corresponding to an average mesh size of 6 km. The vertical density structure is represented by 19 isopycnal layers, topped by an active surface mixed layer that exchanges mass and properties with the isopycnal layers underneath. The mixing parameterization includes a Richardson number dependent diapycnal mixing and entrainment parameterization (Hallberg, 2000; Papadakis et al., 2003). The simulation is initialized from rest and carried out for 6 years.

Many characteristics of the model are similar to a previous MICOM simulation (Paiva et al., 1999; Garraffo et al., 2001*a*,*b*) which was forced with the COADS monthly climatology, and had a slightly different domain configuration (extending to $65°$N, with no Mediterranean Sea). The new simulation shows a better agreement with observations for the Gulf Stream extension, which was previously located about 200 km farther north than what derived from in-situ drifters (Chassignet and Garraffo, 2001). In Garraffo et al. (2001*b*), the numerical results have been quantitatively compared with measurements from surface Lagrangian drifters. The comparison shows that, although the numerical eddy field is less energetic than the in-situ one, the model is able to capture the main circulation features and spatial patterns of the variability. Further studies (Garraffo et al., 2003; Schmid et al., 2003; Foltz et al., 2004) also indicate that the MICOM fields represent properly observed characteristics of coherent structures, such as mesoscale vortices and tropical planetary waves. For these reasons, the model appears suitable to the present study, in which we are mainly interested in understanding the relationship between Eulerian and Lagrangian parameters within strong vortices and in testing a methodology.

During the last year of the simulation, an extensive numerical Lagrangian data set was released, covering the whole computational domain as well as high density transects across the Gulf Stream axis, at the surface and at the depth levels of 700, 1500, and 3000 m. The regularly spaced synthetic floats were seeded on a $1^\circ \times 1^\circ$ grid and had a life span of 6 months. Every month, a new set of drifters and floats were deployed at identical locations. All the simulated trajectories were evolved isobarically at the depth of their deployment by integrating the corresponding isopycnal velocities whenever the floats changed MICOM isopycnal layer. The scheme used to integrate the MICOM field is a fourth-order Runge-Kutta method with a time step of 1 hour, although the positions were recorded every half a day.

The particular Lagrangian data set used in this paper consists of the regularly spaced 700 m floats, which were intentionally released at the same depth as that of the in-situ isobaric floats analyzed in VGRM, so that direct comparison with the observed statistics is possible. The total number of synthetic floats deployed every month amounts to 62856. The "spaghetti" plot of the trajectories during the first month of MICOM simulation is shown in Fig. 1a, while the total number of independent data, n^*, per 1° squared bin is displayed in Fig. 1b. The value of n^* was computed as $n\,\Delta t/2\,T_L$, where n is the total number of data, Δt is the sampling interval, and T_L is the Lagrangian decorrelation time scale, taken equal to 10 days (VGRM; Owens, 1991). We notice that the number of independent data seldom goes below 50, showing an average value of ≈ 200 in the ocean interior, while ranging between 300 and 500 in the Gulf Stream extension and recirculation regions. This means that the amount of Lagrangian data used in this paper is approximately one order of magnitude larger than the in-situ data set analyzed in VGRM.

3 Methodology

This section is dedicated to the description of the method of investigation leading to the results of the present work. The first part describes the definition and estimate of the spin parameter Ω (and of other LS model parameters), together with the definition of the looper and non-looper regimes. The second part of the section presents the methodology used in identifying a region of interest in the southern Gulf Stream recirculation area.

3.1 Spin parameter and flow regimes

The spin Ω considered in this paper and in VGRM has been first introduced in the literature within the framework of LS models (e.g., Borgas et al., 1997; Sawford, 1999). Lagrangian stochastic models describe the motion of particles in turbulent flows using ordinary stochastic equations, where the action of the turbulent field is parameterized as a function of few parameters. In particular, single-particle models of the first order have been used in many applications in physics of the atmosphere and the ocean (e.g., Thomson, 1986; Griffa, 1996; Falco et al., 2000; Berloff et al., 2002; Reynolds, 2002*b*). In these models, particle positions and velocities evolve jointly as a continuous Markovian process. One of the constraints that determine the precise form of the models is the well-mixed condition (Thomson, 1987), stating that a passive tracer uniformly mixed over the domain remains uniformly mixed at all times. For the simplest applications, i.e. for isotropic, homogeneous, stationary, and incompressible turbulence, this condition allows to constraint the drift term in the LS models, although in general it does not determine it uniquely. This non-uniqueness can manifest itself as a "spin" term that induces a mean rotation of the Lagrangian turbulent velocity (Reynolds, 2002*b*).

For the case of linear spin in two-dimensions and assuming that the crosscorrelation $<u'v'>$ is not significantly different from zero (as the VGRM and this paper eddy statistical analyses prove to be), the LS model can be written as

$$\begin{aligned} \mathrm{d}u' &= -u'\,T_{Lu}^{-1}\mathrm{d}t\,-\Omega\,v'\,\mathrm{d}t\,+(2\,\sigma_u^2/T_{Lu})^{1/2}\mathrm{d}\xi_u \\ \mathrm{d}v' &= -v'\,T_{Lv}^{-1}\mathrm{d}t\,+\Omega\,u'\,\mathrm{d}t\,+(2\,\sigma_v^2/T_{Lv})^{1/2}\mathrm{d}\xi_v, \end{aligned} \tag{1}$$

where u', v' are the two components of the Lagrangian turbulent velocity, σ^2 is the velocity variance given by $< u'^2 >$, and the symbol $<>$ indicates an ensemble average process (subscripts u, v stand for either zonal or meridional components). The random increment $\mathrm{d}\xi$ is a Weiner process with independent components, zero mean, and variance equal to Δt. The spin Ω is estimated as (Sawford, 1999)

$$\Omega = \frac{<u'\mathrm{d}v' - v'\mathrm{d}u'>}{2\,\Delta t\ \mathrm{EKE}}, \tag{2}$$

where EKE is the eddy kinetic energy field, equal to $(\sigma_u^2 + \sigma_v^2)/2$. The parameter (2) is interpreted as the particle mean angular rotation during the time increment Δt, and it can be different from zero only when the velocity crosscovariance function is non zero. Particles with non-zero mean spin statistics are associated with spiraling trajectories, oscillatory velocity autocovariance functions, and subdiffusive transport at intermediate times.

In VGRM the parameters of Eqs. (1) have been estimated from the velocities along float trajectories, with T_L computed from the autocovariance statistics, assuming that the autocovariances are described by a first-order two-dimensional LS model, and Ω calculated from the crosscovariance functions after applying (2) (details on the method and parameter error estimates can be found in VGRM, Appendix B). A preliminary assessment of the overall distribution of spin values (and associated errors) computed for each trajectory by VGRM, indicates the existence of two different float regimes, characterized by a threshold $|\Omega| \approx 0.1\,\mathrm{days}^{-1}$, which corresponds to an oscillation time scale $T_w \approx 60$ days. The "non-loopers", characterized by negligible spin $|\Omega| < 0.1\,\mathrm{days}^{-1}$, live in the background flow and exhibit a diffusive behavior. The "loopers", characterized by finite spin $|\Omega| > 0.1\,\mathrm{days}^{-1}$, live in high-energy coherent structures and are usually subdiffusive. Both regimes have been described in VGRM using model (1) and assuming that the spin distribution is approximately bi-modal, with $\Omega = 0$ for non-loopers and finite Ω for loopers.

The regime separation based on the spin threshold provides similar results to the separation based on a more qualitative method introduced by Richardson (1993), which defines a looper as a trajectory which undergoes at least two consecutive loops in the same direction. Quantitative differences between the two methods are due to the fact that the Ω-criterion (in addition to facilitate the processing of a large number of trajectories) takes into account also looping floats which do not exhibit a clear spiraling behavior due, for example, to temporary weakening of the vortex they are embedded in.

3.2 Identification of the region of interest

A general approach similar to the VGRM investigation is followed here in identifying a region of interest based on quasi-homogeneity properties, both in terms of eddy energy content and dynamical features. While the size and geographical position of the quasi-homogeneous subregions considered in VGRM are strongly influenced by the overall data distribution and density, our present region identification can take advantage of two factors. First, the higher amount of more evenly distributed synthetic Lagrangian data allows us to consider a larger and less patchy region than the VGRM areas of interest. Second, the availability of the MICOM predicted Eulerian fields permits to use the additional dynamical argument, with respect to VGRM, in the region identification process.

Specifically, we will choose an area of interest by considering the eddy kinetic energy field obtained from the simulated Lagrangian trajectories, and the temporal evolution of instantaneous MICOM Eulerian fields. We will focus on the southern Gulf Stream recirculation region, which is characterized by energetic coherent vortices and whose results can be compared to the ones obtained by VGRM in two similar Gulf Stream recirculation areas.

3.2.1 Basin-scale mean flow and eddy kinetic energy

The mean flow $\mathbf{U}$ depicted in Fig. 2a is obtained from the MICOM simulated Eulerian field, by averaging grid-point velocities over $1^\circ \times 1^\circ$ spatial bins and over the one-year time period of the MICOM simulation during which the Lagrangian data were seeded. The definition of the mean flow and the choice of the averaging scale used to compute it, are always delicate issues and often the result of a compromise between data density and resolution (Davis, 1991; Maurizi et al., 2004). In order to address this problem, we considered different methods of computing $\mathbf{U}$ and various spatial scales in the averaging procedure, by means of both the synthetic Lagrangian data and the Eulerian velocity fields predicted by the MICOM simulation. The main insight we gained from this investigation is that relatively coarse-averaged mean flow estimates with spatial scales of 1° (from both Lagrangian and Eulerian data) provide stable eddy statistics with respect to estimating $\mathbf{U}$ at higher resolutions (the discussion and details of the mean flow determination are presented in the Appendix).

The 700 m mean flow (Fig. 2a) features a Gulf Stream Current with typical averaged velocities of $25\,\mathrm{cm\,s^{-1}}$ beyond Cape Hatteras, becoming slightly weaker further downstream. The southern (as well as the northern) Gulf Stream recirculation gyre is clearly seen between 62° and 72°W. A North Atlantic Current of $15-20\,\mathrm{cm\,s^{-1}}$ is also present north of 42°N together with a quite strong Labrador Current that meanders around Cape Flemish and the Grand Banks to join the northern branch of the recirculation gyre north of the Gulf Stream axis (e.g., Pickart et al., 1999; Lavender et al., 2000; Schott et al., 2004). Finally, a subsurface western boundary current is found east of the Bahamas Islands (Antilles Current), and its mean flow of $\approx\ 15\,\mathrm{cm\,s^{-1}}$ agrees quite well with earlier observations (Lee et al., 1996). In the Gulf Stream system, the strength of the mean flow appears weaker (about half) than what shown by observations (e.g., VGRM; Owens, 1991; Zhang et al., 2001), while the basic structure is well represented, with the jet separating from Cape Hatteras at the correct latitude (Chassignet and Garraffo, 2001) and the recirculation patterns clearly reproduced.

The mean flow discussed above is subtracted from the total Lagrangian velocities to yield the fluctuation field $\mathbf{u}'$. The eddy kinetic energy field is then computed by spatially averaging $(u'^2 + v'^2)/2$ over 1° squared bins. The EKE distribution, depicted in Fig. 2b, shows the highly energetic regions of the Gulf Stream extension, with EKE values up to $350\,\mathrm{cm^2\,s^{-2}}$ around 37.5°N, 63°W, and of the North Atlantic Current, with EKE ranging between 150 and $250\,\mathrm{cm^2\,s^{-2}}$. The rest of the basin exhibits much lower eddy variability with typical interior EKE $\approx 20\,\mathrm{cm}^2\,\mathrm{s}^{-2}$. When comparing these results to in-situ observations (VGRM; Owens, 1991; Zhang et al., 2001) we notice that the MICOM eddy kinetic energy underestimates the observed eddy variability up to a factor of two in specific regions such as the Gulf Stream extension area. This is consistent with previous findings for the modeled ocean surface (Paiva et al., 1999; Garraffo et al., 2001*b*).

3.2.2 Evolution of instantaneous MICOM fields

In order to characterize and identify coherent structures in the MICOM solution, we consider three different diagnostic fields. The first one is the velocity amplitude of the instantaneous Eulerian flow, $|\mathbf{u_E}| = \sqrt{u_E^2 + v_E^2}$ (where the subscript is used to distinguish this field from the Lagrangian velocity), which provides a direct identification of the high energy features and mechanisms, such as jet meandering, Gulf Stream ring's shedding and Gulf Stream-eddy interactions. The second diagnostics is provided by the relative vorticity, computed from $\mathbf{u_E}$ as $\zeta = \partial v_E/\partial x - \partial u_E/\partial y$, which identifies regions characterized by strong horizontal shear and by the presence of coherent vortices. Finally, the distribution of the Okubo-Weiss parameter (Weiss, 1991), Q, has been considered. This quantity is often used in two-dimensional turbulence to describe the relative importance of vorticity with respect to the deformation rate of material lines (e.g., McWilliams, 1984; Elhmaidi et al., 1993). It is given by $Q = d^2 - \zeta^2$, where ζ is the relative vorticity field and d is the deformation (strain) rate whose squared value is defined as

$$d^2 = \left(\frac{\partial u_E}{\partial x} - \frac{\partial v_E}{\partial y}\right)^2 + \left(\frac{\partial v_E}{\partial x} + \frac{\partial u_E}{\partial y}\right)^2 .$$

Since Q typically assumes highly negative values inside coherent vortex cores while it becomes highly positive in the area immediately surrounding the vortex cores (due to the high degree of straining of material lines in that area), this parameter is very useful in identifying vortices and rotating structures.

The time evolution of the three diagnostics during the one-year simulation has been considered. A snapshot of the distribution of $|\mathbf{u_E}|$, ζ, and Q is shown in Fig. 3 (upper, middle, and lower panels, respectively). Considering that the MICOM Eulerian fields at 700 m were recorded every 3 days, a total of 120 frames of the kind depicted in Fig. 3 were observed evolving during the one-year simulation period. A close-up movie depicting the evolution of $|\mathbf{u_E}|$ and a sample of looping trajectories trapped inside the simulated Gulf Stream rings, can be seen online at http://www.rsmas.miami.edu/LAPCOD/research/ 2004d/ampl_trajs.06-20b.gif.

The main dynamical features that are identified in the Gulf Stream area are outlined in the following, with an emphasis on the coherent vortices forming and evolving in the southern recirculation region.

- The Gulf Stream obviously dominates the energetic scene, undergoing strong meandering and ring's shedding, both to the north and to the south of the jet axis. During the one-year simulation, a total of 7 cold-core (cyclonic) Gulf Stream rings are identified, of which 5 are actually formed during the one-year period, yielding a formation rate comparable with averaged observed values (Richardson, 1983). The modeled cold-core rings start migrating west-southwestward as soon as they detach from the Stream with translation speeds of $\approx 4 - 6\,\mathrm{cm\,s^{-1}}$. Their size, measured as the radius of maximum velocity, varies between 40 and 80 km. All these characteristics, except for the ring's energy, are similar to typical observed features (e.g., Vastano et al., 1980; Joyce, 1984; Brown et al., 1986; Chassignet et al., 1990; Olson, 1991).

- Various ring-stream interactions take place, not only during the ring formation process but also later along the migrating path, especially when the Gulf Stream undergoes strong meandering events.

- Mainly because of these interactions, rings tend to change their intensity during their life, typically strengthening at the time of the interaction but subsequently weakening after the event has taken place. In two cyclonic ring cases such events are fatal for the ring because the vortices are reabsorbed by the jet, while in one case the cold-core ring almost disappears for several days only to reform as a new coherent vortex westward of its latest location. Ring-ring interactions are also strong, with two clear cases of cyclonic rings merging into each other.

- The eastern region of the Gulf Stream recirculation appears to be more influenced by wave fields, although rings and other coherent vortices are still present. In particular, one anticyclone is identified forming a dipole with a Gulf Stream cold-core ring for a 1.5-month period, then detaching and migrating eastward before weakening and fading into the background flow.

3.2.3 Region of interest

On the basis of the eddy energy content and dynamical characteristics discussed in sections 3.2.1 and 3.2.2, we choose our region of interest located in the southern Gulf Stream recirculation area between $52°$ and $72°$W. The region features an abundance of cyclonic cold-core rings, yet remaining at a certain distance from the Gulf Stream axis in order to exclude the highly non-linear and non-stationary areas where frequent ring-stream interactions take place.

The area of interest, hereafter referred to as RINGS, is contoured in Fig. 4, superimposed on the mean circulation $\mathbf{U}$ (upper panel), the eddy kinetic energy field (middle panel), and a snapshot of MICOM velocity magnitude $|\mathbf{u_E}|$ (lower panel). The region consists of two recirculation cells. A western cell, extending zonally between $62°$ and $72°$W and meridionally between $34°$ and $36°$N, is characterized by a clear recirculation mean flow of $5 - 10\,\mathrm{cm\,s^{-1}}$, and an eastern cell, extending between $52°$ and $62°$W and between $35°$ and $38°$N, exhibits a weaker but still recirculating mean field of up to $5\,\mathrm{cm\,s^{-1}}$. The whole RINGS area is characterized by a quasi-homogeneous eddy kinetic energy of $\approx 70\,\mathrm{cm^2\,s^{-2}}$. As for the dynamical features, the region is dominated by the presence of coherent vortices, in particular 5 cyclonic cold-core rings enter the area after being shed from the Gulf Stream and migrate west-southwestward following the recirculation mean flow. An anticyclone is also present for about two months in the eastern part of RINGS, first migrating westward and coupling with a Gulf Stream ring, then detaching and migrating eastward before disappearing in the background flow.

The direct effect of these coherent vortices is to produce two distinct categories of MICOM simulated trajectories, the loopers and non-loopers, similar to those observed from in-situ floats (VGRM; Richardson, 1993). Here, the looping trajectories are separated from the non-loopers using the same spin-based criterion introduced in VGRM and described in section 3.1, for which a trajectory is consider a looper if its overall $|\Omega|$ is higher than the $0.1\,\mathrm{days}^{-1}$ threshold. A sample of MICOM loopers is shown in the lower panel of Fig. 4 where the rings responsible for their looping behavior are also visible. By taking into account only trajectories longer than 15 days, a total of 76969 simulated float days are available in RINGS, out of which 56771 are non-loopers

(73.8%), 16176 are cyclones (21.0%), and 4022 are anticyclones (5.2%). Such a distribution is in good agreement with the distribution of loopers and non-loopers found in VGRM from in-situ floats inside the two Gulf Stream recirculation subregions RECW and RECE, where the number of loopers amounted to 23% of the total float population.

4 Lagrangian data analysis and comparison with observations

4.1 Results

The MICOM Lagrangian data have been analyzed following the same general methodology as in VGRM. The eddy statistics obtained from the fluctuation field $\mathbf{u}'$ are characterized in terms of Lagrangian velocity autocovariance and crosscovariance functions, considering both the complete data set and the separated subsets of the looping and non-looping trajectories. A quantitative evaluation of the Lagrangian parameters, such as the decorrelation time scale T_L and the spin Ω, is also performed by applying the VGRM method described in section 3.1.

It should be noticed that an initial data treatment has been carried out for the looping floats, aimed at correctly removing the average propagation speed of the coherent structures which the loopers were embedded in. The reason for the treatment (which was not performed in VGRM because of the more restricted sampling) is that a persistent positive shift was observed in the loopers zonal autocovariance function, suggesting that the average propagation was not correctly removed. The original looping trajectories have been first smoothed by averaging positions over 60-day periods, in order to isolate the mean propagation from the rotational motion, and then the smoothed velocities have been computed and averaged. Best results are obtained by averaging separately over the two cells comprising region RINGS.

The translation speed $\mathbf{U_t}$ of the cyclonic trajectories is mostly westward in the western cell (with values $U_t,\, V_t = -4.8,\, -0.6\,\mathrm{cm\,s^{-1}}$), while it has a relatively more pronounced southward component in the eastern cell ($U_t,\, V_t = -1.8,\, -0.9\,\mathrm{cm\,s^{-1}}$). This is consistent with what shown by the Eulerian field evolution [2] and with the main Eulerian features outlined in section 3.2.2. Anticyclonic floats are only present in the eastern part of RINGS and since they represent only 5.2% of the total Lagrangian data, their statistics do not contribute significantly to the overall loopers behavior. Further checks have been performed to verify that the loopers statistics were constant over the two cells (as implicitly assumed by considering RINGS as a single region), and indeed the covariance functions and the typical time scales were found to be independent from the particular cell and well defined over the entire region.

Velocity autocovariance and crosscovariance functions are shown in Fig. 5 for the complete Lagrangian data set and separately for the non-loopers and the cyclonic floats (anticyclonic trajectories are not included because of their insignificant contribution to the loopers statistics). The overall zonal autocovariance function (Fig. 5a) exhibits a first positive lobe more pronounced than the first negative lobe at $t \approx 20$ days. As in VGRM, we interpret this feature as due to the superposition of the two different eddy regimes described by the non-loopers and loopers autocovariances shown in Fig. 5b and 5c, respectively. The non-looping float statistics (Fig. 5b) are mostly diffusive with approximately exponential autocovariance functions (except for the initial time lags), and significant anisotropy between the zonal and meridional components. This asymmetry has been noted before in float data (e.g., Freeland et al., 1975; LaCasce and Speer, 1999), and it is likely to be

[2] movie at: http://www.rsmas.miami.edu/LAPCOD/research/2004d/ampl_trajs.06-20b.gif.

related to the inhibiting effect of differential earth rotation (β) in the meridional dispersion. In our case, this effect might be partially enhanced by the shape of the selected region of interest, which is more elongated in the meridional direction than in the zonal one, therefore introducing a possible bias in the considered particle displacement. The non-loopers crosscovariance functions (Fig. 5e) are approximately flat, suggesting that the non-looping MICOM floats are associated to a very low value of the spin parameter Ω. Cyclonic trajectories, on the other hand, are more energetic and characterized by strong oscillatory autocovariance function (Fig. 5c) with a marked first negative lobe and well defined non-zero crosscovariances (Fig. 5f). This behavior is clearly indicative of rotational motion, with trajectories trapped inside coherent vortices associated to a finite value of spin Ω.

Quantitative estimates of Ω, variance σ^2 and Lagrangian time scale T_L (both zonal and meridional), and space scale r obtained from the non-looping and the cyclonic floats are provided in Table 1. The cyclonic loopers are significantly more energetic than the non-loopers (≈ 3 times as much), while T_L values are similar for looping and non-looping trajectories ranging between 12 and 15 days. The spin assumes a very small value for non-loopers as expected from the behavior of the crosscovariance functions, while it is approximately equal to $0.21\,\mathrm{days}^{-1}$ for cyclonic floats, corresponding to an oscillation time scale $T_w \approx 30$ days. These estimates reflect the "average" values of the parameters and they could be used in a similar fashion as in VGRM to implement a bi-modal LS model of the kind described by Eqs. (1).

In order to gain more insights into the actual distribution of the parameter values, we consider the scatterplot of Ω versus EKE computed by averaging over single trajectory records longer than 60 days (values computed from shorter trajectories are not included because they can be too noisy).

The results, which are depicted in Fig. 6, are similar to those (not shown) obtained when changing the averaging method, for instance when Ω and EKE are running averaged over 60-day periods along the trajectories. As it is clear from Fig. 6, the majority of the trajectories ($\approx 80\%$ of the data) lies in a cluster characterized by $|\Omega| < 0.1\,\mathrm{days}^{-1}$ and EKE $< 100\,\mathrm{cm}^2\,\mathrm{s}^{-2}$, corresponding to the non-looping regime. The loopers, characterized by $|\Omega| > 0.1\,\mathrm{days}^{-1}$, are mostly cyclonic and they are associated to an average value of $\Omega \approx 0.24\,\mathrm{days}^{-1}$, consistently with the results of Table 1. A significant scatter can be seen in the loopers Ω and EKE values, with Ω ranging between 0.1 and $0.4\,\mathrm{days}^{-1}$ and EKE varying between 40 and $280\,\mathrm{cm}^2\,\mathrm{s}^{-2}$. The reasons for this behavior and its relationship with the Eulerian properties of the flow field will be investigated in section 5.

4.2 Comparison with observations from VGRM

A qualitative comparison with the VGRM results is carried out focusing mostly on loopers and coherent structure features. We consider the two VGRM regions, RECW and RECE, which are situated in the southern Gulf Stream recirculation area and are partially overlapping with RINGS. Region RECW is located in the western part of the recirculation, ranging zonally between $64°$ and $72°$W and meridionally between $32°$ and $35°$N, therefore being partially shifted to the south and more distant from the Gulf Stream axis with respect to RINGS. Region RECE is in the eastern part of the recirculation, between $43°$ and $62°$W and between $34°$ and $37°$N, therefore extending further eastward than RINGS.

The autocovariance functions for RECW and RECE are reported from VGRM and shown in Fig. 7. A qualitative comparison with the corresponding MICOM results (see Fig. 5) reveals that the basic features of the eddy statistics are similar to those predicted by the synthetic floats. In particular, the overall in-situ data autocovariances (Fig. 7a,d) show a pronounced first positive lobe and this behavior appears to be due to the superposition of the regimes associated with the looping and non-looping trajectories. Furthermore, non-loopers are mostly diffusive (Fig. 7b,e), with a more marked anisotropy in RECE, while loopers give rise to oscillating autocovariances (Fig. 7c,f). The crosscovariance functions (not shown, see Figs. 5 and 8 in VGRM) also have a similar behavior to the one exhibited by the MICOM float statistics, with values non-significantly different from zero for non-loopers and well defined oscillatory patterns for loopers.

A more quantitative comparison reveals that the main differences between in-situ and simulated data statistics is in terms of energy content, in agreement with what described in section 3.2.1 from the pseudo-Eulerian eddy field and with previous results from surface drifters (Garraffo et al., 2001*b*). While Garraffo et al. (2001*b*) also found that the MICOM Lagrangian time scales overestimate the real values, possibly because of the lack of synoptic variability in the model external forcing, here we find less evident discrepancies in terms of time scales. Lagrangian decorrelation scales T_L in RECW and RECE range between 7 and 12 days, being less than half of the corresponding estimates in RINGS ($12 - 15$ days). This could be due to the fact that the present and VGRM eddy analyses are carried out at 700 m, i.e. at a depth where direct influence from surface forcing is somehow limited. Regarding the comparison between in-situ and MICOM predicted oscillation time scales, in region RECW loopers are characterized by $T_w \approx 10$ days, showing a significant difference with the MICOM loopers $T_w \approx 30$ days. It is important to notice, however, that the RECW statistics are highly influenced by the presence of two very energetic anticyclones which lived in the region for periods of up to 6 months (see Ω-EKE scatterplot in VGRM, Fig. 16). These anticyclones are likely to be subsurface warm lenses whose formation mechanism has not been completely clarified but thought to be related either to the detachment of 18° Water patches during extremely cold winters (Brundage and Dugan, 1986), or to interactions with the Corner Rise seamounts (Richardson, 1980). Occurrence of such strong events is relatively rare, and it is therefore not surprising that they were not predicted by the MICOM climatological single year simulation.

In region RECE, on the other hand, the looper oscillation time scale is approximately 18 days and therefore closer to the MICOM estimate. The looper statistics are also dominated by cyclonic trajectories as in RINGS, most probably due to the presence of Gulf Stream rings. When considering the RECE autocovariance statistics (Figs. 7d–f), the oscillation patterns have a structure suggestive of the superposition of a limited number of coherent structures characterized by different time scales. This is confirmed by the Ω-EKE scatterplot (Fig. 16 in VGRM), which shows the existence of a few particularly long living loopers exhibiting different values of EKE and Ω. In other words, the Ω-EKE scatterplot for RECE resembles a decimated version of the corresponding MICOM plot (Fig. 6). Despite this sampling problem and as noted above, the estimated parameter values are significantly closer to the MICOM results than those in RECW. The observed discrepancies in terms of Ω and T_w values can be mostly a consequence of the differences in eddy energy. In fact, considering that MICOM rings exhibit similar spatial scales to the observed structures as discussed in section 3.2.2, an overestimate of the model oscillation time scale on the order of $\sqrt{2}$ is expected as a result of the MICOM underestimate by almost a factor of 2 of the eddy kinetic energy levels.

Summarizing, in spite of some quantitative differences with observational results, the MICOM solution is able to capture the main characteristics of the flow. A clear distinction is found, as in the in-situ data, between loopers and non-loopers, confirming the existence of the two separated regimes associated with vortices and background flow. Apart from eddy energy levels, the looper characteristics for cyclonic vortices are in a similar range for observed and simulated trajectories, in agreement with the assessment of section 3.2.2 on the Eulerian characteristics of rings, in terms of formation rate, mechanisms, and propagation. In conclusion, the comparison confirms that the model flow is adequate to the present study, focused on the relationship between Lagrangian and Eulerian properties in coherent structures.

5 Lagrangian spin estimates and the Eulerian vorticity field

The Lagrangian physical meaning of the spin parameter Ω has been discussed in section 3.1 and associated with the mean angular velocity of the particle velocity vector. Its relationship with the underlying Eulerian flow structure, on the other hand, remains to be investigated and it is the focus of the present section. In particular, we are interested in verifying whether the Lagrangian Ω estimate (2) for loopers can be used to quantitatively characterize the Eulerian vorticity ζ of the underlying rings. In the following, we discuss in which circumstances we can expect this to occur and what are the corresponding physical implications.

The general expression of relative vorticity ζ in polar coordinates, r, θ, is given by

$$\zeta = \frac{v_\theta}{r} + \frac{\partial v_\theta}{\partial r} - \frac{1}{r}\frac{\partial v_r}{\partial \theta}, \tag{3}$$

where v_r and v_θ are the radial and tangential velocities, respectively. Observations suggest (e.g., Olson, 1980) that the relative vorticity within rings is primarily due to the streamline curvature and to the shear of the tangential velocity v_θ,

$$\zeta \sim \frac{v_\theta}{r} + \frac{\partial v_\theta}{\partial r}.$$

In the ring's core this expression is expected to further simplify due to the fact that v_θ increases approximately linearly with the distance from the ring's center, i.e. that $v_\theta \sim \Omega_E\, r$, where the Eulerian angular velocity Ω_E is a constant value. This is equivalent to say that the vortex core is approximately in solid body rotation (e.g., Olson, 1980; Joyce, 1984), and it implies that the relative vorticity expression becomes simply $\zeta \sim 2\Omega_E$.

If the loopers are sampling the vortex core, the angular velocity Ω_E is expected to coincide with the Lagrangian spin Ω, suggesting that the following relationship holds

$$\zeta \sim 2\Omega. \tag{4}$$

Summarizing, the validity of (4) depends on two main physical assumptions: a) that the vortex core is in solid body rotation, and b) that the loopers significantly sample the core against the outer part of the vortex. In the following we will directly verify whether (4) holds for the 5 rings that form and propagate during the one-year MICOM simulation in which Lagrangian particles are seeded. If the results are positive, this will implicitly indicate that the two physical assumptions a) and b) are also valid.

For each ring, the complete instantaneous relative vorticity (3) is estimated and followed in time during the period spent by the ring inside region RINGS. The estimate of ζ in the ring's core is performed by spatially averaging the MICOM vorticity field in the region around the ring's center, defined as the area where ζ values are within 20% of the vorticity of the vortex center. The temporal evolution of the instantaneous $\zeta/2$ is then compared with that of the Ω values computed considering the looping trajectories that surround or are embedded inside the ring's structure, and using a 60-day running average version of (2). To facilitate the comparison, also 60-day running averages of $\zeta/2$ are calculated.

Three specific examples of ring evolution are shown and discussed in detail, while the overall results for the 5 rings are summarized in Table 2. Rings are numbered in progression as they are formed during the MICOM simulation. Rings 02 and 05 are also characterized by two letters, A and B, indicating distinct ring's stages that correspond to before and after strong interactions with the Gulf Stream, during which the ring's structure is no longer recognizable.

The three cold-core rings discussed in details are 04, 01, and 05A-B. They have been chosen because they represent significant examples of ring's evolution, with rings 04, 01 migrating westward mostly undisturbed, and ring 05 experiencing a more dramatic history and a strong interaction with the Gulf Stream before continuing to translate south-westward. A snapshot of the ring 04 vertical structure is shown in Fig. 8 (similar structures are found for the other two rings). The upper two panels depict the contours of meridional (zonal) Eulerian velocity along a zonal (meridional) ring's vertical cross section, superimposed on the MICOM isopycnal layers, while the lower two panels show the vertical profile of the ζ field along the same ring's sections. The velocity profiles indicate that there is a maximum swirling flow at ≈ 50 km from the ring's center. Also evident is the fact that the relative vorticity field remains approximately constant at 700 m depth inside the ring's core, within the radius of maximum velocity, as hypothesized above.

The time evolution of Eulerian vorticity $\zeta/2$ and Lagrangian spin Ω for a significant sample of trajectories looping inside the ring's structure, are illustrated in Fig. 9a for ring 04. In total there are 11 loopers associated with ring 04, of which 7 are shown here. The ring forms around simulation day 75 (days are counted with respect to the first seeding time of the MICOM Lagrangian data), but starts influencing substantially the RINGS region only later, migrating westward along the RINGS western cell and merging with a second ring (01) between day 210 and 219. Towards the end of its life (day $230 - 280$) the ring is observed interacting strongly with the Gulf Stream and merging with a third cold-core ring (02A-B), before the whole structure is completely reabsorbed by the Stream outside the RINGS region. This vortex history can be followed quite accurately through the changes in $\zeta/2$ (thick black line in Fig. 9a). The vorticity oscillates slightly around a constant mean value of $\zeta/2 \approx 0.3\,\mathrm{days}^{-1}$ during most of the ring's life, with oscillations mainly representing weak interactions with the Gulf Stream, while it undergoes more substantial variations in connection with the ring-ring interactions and merging processes (strong decrease in $\zeta/2$ around day 220 and subsequent strong oscillation event). The 60-day running average of $\zeta/2$, indicated by the red line in Fig. 9a, is smoother and it shows a slight delay with respect to the instantaneous vorticity pattern.

Lagrangian Ω values computed over 60-day periods along the loopers (thin black lines) appear to represent quite well the ring's vorticity (or the angular velocity Ω_E). This is especially clear when comparing the spin with the 60-day running average version of $\zeta/2$ (red line), which shows a close similarity with the Ω evolution of the majority of loopers. There is only one case of trajectory that appears different from the others, providing a significant lower value of Ω around day 210. This is most probably due to the fact that the float is sampling the edge of the ring rather than its core.

While the trajectories shown in Fig. 9a are only a sample of the complete looper ensemble in ring 04, they represent quite well the overall situation, which is summarized as follows.

- Most of the looping trajectories (85%) are core-loopers, i.e. they remain trapped inside the radius of maximum swirling velocity and within the area where relative vorticity is highly positive and approximately constant. These core-loopers are responsible for the very good estimates of ring's vorticity seen in Fig. 9a. One example of such trajectories in physical space is shown in Fig. 9b as a thick solid line superimposed on a snapshot of the Eulerian vorticity field.

- The remaining loopers (15%) tend to sample the edge of the ring's core, and they are usually shorter-living than core-loopers because they are not efficiently trapped inside the coherent structure. These loopers yield an underestimate of the ring's vorticity perhaps because they live in the area around the vortex where the hypothesis of solid-body rotation starts breaking down.

- Finally, a number of floats surround the ring's structure only temporarily, subsequently leaving the vortex area rather quickly. Their looping regime is so short that they yield an overall estimate of Ω which is non-significant, i.e. they behave overall as non-loopers. This is probably due to the high degree of deformation rate of material lines that is observed outside the ring's core (see Okubo-Weiss parameter, Q, in Fig. 3), which makes it difficult for particles to reside in that area for long periods of time (e.g., Provenzale, 1999). One such float example is the dashed trajectory pattern in Fig. 9b.

While the results of ring 04 clearly indicate that Ω values are related to the ring's core vorticity, the relatively weak dependence on time of ζ does not allow to verify how closely the temporal evolution and history of $\zeta/2$ are followed by the evolution of Ω. In order to assess this point, another example of ring evolution is considered, characterized by a more marked time-dependence.

In Fig. 10 the history of $\zeta/2$ for ring 01 is shown (instantaneous values are again indicated by a thick black line). Ring 01 is already present at the time when MICOM floats start being seeded, and it is initially located at the eastern end of the RINGS western cell. For about 8 months, the vortex migrates steadily westward along the region, finally interacting and merging with ring 04. Weak interactions with the Gulf Stream also take place, producing intermittent strengthening events but never altering the coherent structure of the ring. An increase in the average $\zeta/2$ (red line) is evident.

As it can be seen from the pattern of the thin black lines in Fig. 10, the Lagrangian Ω values of a sample of loopers located within the ring's core (4 of the total 9 loopers are shown) follow the temporal changes of the Eulerian $\zeta/2$ very well, especially in correspondence of the raise in vorticity between day 140 and 160.

Qualitatively similar results are found for ring 05A-B, except that in this case the situation is complicated by the occurrence of a major interaction between the ring and the Gulf Stream which introduces substantial variations in the ring's structure. Ring 05A starts affecting the region eastern cell at day 180, it migrates westward during the subsequent 2 months before a temporary merging with the Stream takes place. The vortex loses its coherence for a number of days, only to reappear, as ring 05B and slightly weaker than before, south-westward of its latest location. The ring then continues translating westward in the RINGS western cell.

Such dramatic history is reflected in the ring's vorticity evolution depicted in Fig. 11a, which shows an initial $\zeta/2$ characterized by a mean value of $\approx 0.35\,\mathrm{days}^{-1}$, while featuring a lower core angular velocity of $\approx\ 0.28\,\mathrm{days}^{-1}$ after the strong ring-stream interaction has occured between day 245 and 270. Results in terms of Lagrangian spin values (6 of the total 22 loopers are shown in Fig. 11a) are qualitatively similar to those obtained for rings 04, 01. Core-loopers are found to be the majority of the looping floats, and most of them provide good estimates of the ring's vorticity and angular velocity Ω_E, especially before day 245. Spin values drop substantially after the ring's temporary disappearance into the Gulf Stream, down to a point where some of them enter the non-looper regime ($\Omega < 0.1$). In one case, the float lives long enough to show that the looper to non-looper transition is followed by an opposite transition event during which the Lagrangian spin increases back to looper-regime levels. This specific trajectory is shown in Fig. 11b,c, superimposed on snapshots of the Eulerian relative vorticity field (panel b illustrates the looper regime stage associated with ring 05A, while c shows the non-looper to looper transition and the subsequent looping pattern associated with the ring's weakening and restrengthening as ring 05B). The Ω values computed during the second stage of ring 05 tend to be lower than the Eulerian $\zeta/2$ values. This is attributed to two possible reasons, i.e. to the breaking down of the hypothesis of solid body rotation within the core due to the major coherent structure disruption event, and to the fact that loopers are sampling the ring's edge after this event.

Overall results for each of the 5 rings are summarized in Table 2, in terms of mean $\zeta/2$ and Ω, and in terms of total number of loopers and transition events taking place between looper and non-looper regimes and vice versa. The mean Eulerian vorticity is computed by averaging the instantaneous values in time (over the whole temporal evolution), while the mean Ω is estimated by averaging both in time and over the whole looper ensemble for the specific ring. It is clear from these results that the looper Lagrangian spin Ω provides a very good estimate of the Eulerian ring's core vorticity. The only evident discrepancy is found for ring 05, which is also the ring experiencing the most dramatic evolution, as discussed above. Furthermore, the presence of a high number of transiting trajectories (which is absent in ring 02 because of the large temporal separation between the A and B stages of this ring) yields Lagrangian spin values that are intermediate quantities between the looper and non-looper regimes, thus underestimating the overall Ω_E over the considered evolution period.

The investigation allows to assess the reasons for the scattered values of Ω observed in the Ω-EKE plot of Fig. 6 (and most probably for the similarly scattered values seen in RECW and RECE from the in-situ data analysis, Fig. 16 in VGRM). Since Ω follows the vortex history fairly well, it tends to change when the vortex structure actually changes in time (mainly as a consequence of ring-stream and ring-ring interactions). Furthermore, intermediate values of Ω between the looper and non-looper regimes are due to transition events which the particle undergoes when the vortex they are embedded in experiences strong structure changes (temporary or permanent reabsorption in the Gulf Stream). Similar reasons for the scattered values of EKE in Fig. 6 are envisioned. Moreover, while Ω is approximately constant within the vortex core, the energy increases from the vortex center to the radius of maximum velocity, so that even slight radial migrations of the float inside the core produce scattered values of EKE.

The overall results permit, on the one side, to attribute a specific Eulerian physical meaning to the Lagrangian spin Ω, and, on the other, to provide an alternative means of estimating the vorticity field of coherent vortices, a quantity more difficult to compute otherwise. As already mentioned, this outcome also implies that the two following physical assumptions are valid: a) that the vortex core remains in solid-body rotation during its evolution, and b) that the looping particles persistently sample the vortex core rather than its edge. The first assumption, in agreement with previous experimental results (e.g., Olson, 1980; Joyce, 1984), has also been directly tested considering an independent estimate of the ring's core angular velocity, which consists in computing the slope of the Eulerian velocity profiles, inside the core, along 4 ring's radial cross sections (zonal, meridional, and two diagonal sections). The mean Ω_E over the 4 sections was calculated and its time evolution compared with that of the $\zeta/2$ estimates. Similar patterns were found between the two quantities (except during very strong ring-stream interactions as found for rings 02, 05) for all the 5 cold-core rings present in the RINGS region. The second assumption is verified by the high percentage of core-loopers found in the MICOM simulated rings. This assessment is also in agreement with results of two-dimensional turbulence dynamics, which identify vortex cores as highly trapping features for Lagrangian particles and the areas immediately surrounding the core as regions where particles tend to spread towards the background flow field (Elhmaidi et al., 1993; Provenzale, 1999).

6 Conclusions and future developments

In this paper, an analysis of the Lagrangian spin parameter Ω and its relationship with the Eulerian flow field in the presence of strong coherent vortices is presented. The use of numerical Lagrangian trajectories released in a high-resolution Ocean General Circulation Model (OGCM) allows to overcome the problem of limited in-situ data, on the one hand, and to utilize additional information on the OGCM-simulated Eulerian flow field, on the other.

The focus is on the southern Gulf Stream recirculation region characterized by quasi-homogeneous eddy energy and by the presence of mesoscale coherent vortices, mainly Gulf Stream cold-core rings. Lagrangian statistics in terms of velocity autocovariance and crosscovariance functions and eddy parameters are computed and discussed in the area of interest.

The study is successful in confirming the VGRM result that the eddy field can be thought of a superposition of two separated regimes. One regime is associated with coherently rotating vortices which give rise to looping trajectories exhibiting subdiffusive behavior due to the trapping effect of the vortices, while the other regime is associated with the background eddy flow and produces non-looping floats.

The strength of this work, however, is having established a clear relationship between the Lagrangian spin parameter Ω for loopers embedded inside coherent vortices and the Eulerian vorticity field ζ of the vortices. The majority of looping floats analyzed here, in fact, live inside the coherent vortex core, providing estimates of Ω that are very comparable with the vorticity and angular velocity field evaluated from the Eulerian flow structure. Furthermore, the time evolution of the core-looper Ω values follows the history of the vortex vorticity, suggesting that spin estimates obtained from a sufficiently high number of looping trajectories can be used as a proxy for ζ. These results consolidate and complete the VGRM investigation, allowing to address the open issues concerning the Eulerian physical meaning of Ω. Even more importantly, this and the VGRM work lead to the introduction of an excellent general methodology to identify the coherent vortices and separate looper and non-looper regimes from Lagrangian data through the Ω parameter. The present study can be extended to other regions of the world ocean, so that the importance of mesoscale coherent vortices in the eddy transport characteristics of passive tracers can be assessed on a broader geographical scale.

In order to achieve this purpose, further investigations are needed to explore the effects of the vortices on the particle dispersion properties and to provide an appropriate description of the results through suitable Lagrangian stochastic models. Such issues are being addressed and will be part of a forthcoming publication.

A final comment must be made here to point out that the link between the Lagrangian spin and the Eulerian vorticity was demonstrated for particular dynamical features, that are the coherent, water mass trapping, mesoscale vortices. Further investigation is needed to understand the meaning of Ω in dynamically different coherent structures, such as the highly sheared unstable jets and the large scale wave fields.

Acknowledgments. The authors are thankful to Bill Johns, Arthur Mariano, Don Olson, Tamay Özgögkmen, and Andy Reynolds for numerous stimulating discussions, and to Leonid Piterbarg for suggestions on statistics and error estimates. They also thank Greg Holloway for his careful reading of the manuscript and helpful comments. Ed Ryan did a great job in editing the MICOM velocity movie and Paolo Erdman in posting it on the web. This research was supported by the National Science Foundation through grant OCE-9811358. A. Griffa also acknowledges the support of the Office of Naval Research through grant N00014-97-1-0620. M. Veneziani wishes to thank Gennaro for the enormous support given during her PhD Dissertation work, but mainly for being there by her side. This work has benefited from the very constructive comments and suggestions of the two anonymous reviewers.

APPENDIX

Estimate of the mean flow

A primary task to be carried out when studying problems related to the eddy fluctuation field, $\mathbf{u}'$, consists in computing an accurate estimate of the mean flow, $\mathbf{U}$, that must be subtracted from the total velocity field to yield $\mathbf{u}'$. The mean flow should be representative of the large scale dynamics with time scales longer than the mesoscale, and should possibly solve horizontal shears of strong currents and jets. The choice of the averaging scale used to compute $\mathbf{U}$ is a delicate issue and usually a compromise between the need of an adequate mean flow and the necessity of keeping the data density high enough to ensure the statistical significance of the results (Davis, 1991; Maurizi et al., 2004). The problem has been addressed in this paper by performing a thorough investigation considering different methods of computing $\mathbf{U}$ in order to test the robustness of the eddy statistics with respect to the particular estimate of the mean flow. The availability of both the MICOM simulated Lagrangian data and the modeled Eulerian flow field has allowed for the computation of independent estimates of $\mathbf{U}$ and for the assessment of the results by using more and more refined spatial scales in the averaging process.

First, the estimate of $\mathbf{U}$ has been performed from Lagrangian data, similar to what carried out by VGRM. Previous investigators have adopted a number of methods to either average or interpolate the velocity field along the trajectories, yielding an Eulerian distribution in space and time of the mean circulation ("pseudo-Eulerian" field). A commonly used method is the "binning technique" (e.g., Poulain and Niiler, 1989; Owens, 1991), through which the float velocities are averaged over small spatial subregions (bins) and over a certain period of time. The bin size is generally chosen as a trade-off between the importance of resolving both spatial shears of the mean flow and eddy scales on the order of the internal Rossby radius of deformation, and the necessity of keeping a high enough data density to guarantee statistical significance of the results. Alternative Lagrangian methods include objective mapping (Davis, 1998) or bi-cubic spline interpolation techniques (Bauer et al., 1998). The spline interpolation of the Lagrangian velocities, which was used successfully in VGRM, depends on four parameters, the knot spacing and three weights associated with uncertainties in the data and in the first and second derivatives of the interpolated field (Inoue, 1986; Bauer et al., 1998). In our analysis, we have first considered the $1^\circ \times 1^\circ$ binned mean flow. Then, we have computed various spline interpolated fields by varying the spline parameter called roughness, ρ, which is related to the second derivative of the splined flow and controls the wavenumber content of the results. We have performed a sensitivity analysis by varying the roughness in the range $10^{-2} - 1000$, changing its value by one order of magnitude at a time. It has been found that, for all the roughness choices, the eddy statistics tend to asymptote at high values of ρ, with the shape of the autocovariance and crosscovariance functions becoming independent from the specific value of roughness. Furthermore, the statistical results do not change significantly when considering the binned mean flow, suggesting that the eddy statistics are robust.

Second, the estimate of the mean flow has been performed from the Eulerian MICOM velocity field, by averaging the velocities over spatial bins and over the one-year time period during which the Lagrangian data were simulated. In this case, the spatial bin can be changed and decreased much further with respect to Lagrangian estimates, given the high resolution of the model, allowing for a direct assessment of the effect of coarse averaging scales on the definition of the mean flow. We changed the spatial scale of the averaging process by considering first a bin size of 0.1°, that is on the order of the MICOM horizontal resolution, and then by increasing it to 0.5° and 1°. The three different mean flow fields are found to produce an eddy fluctuation field characterized by very similar statistics, in terms of autocovariance and crosscovariance functions. Furthermore, the eddy statistics are very similar to the results obtained by using the Lagrangian based mean flow. This is an important achievement because it suggests that $\mathbf{U}$ estimates based on a 1° bin average, which are commonly performed with in-situ data (e.g., Owens, 1991; Bracco et al., 2000*a*; Fratantoni, 2001), are appropriate and lead to robust eddy statistics (provided that the data density is sufficiently high inside the bins).

The mean flow used to draw most of the eddy statistics presented in this paper is the annual Eulerian MICOM field averaged over 1° squared bins. As discussed in section 4.1, a different investigation was carried out for the looping trajectories, in which not the mean flow but the estimated vortices translation speed was subtracted from the loopers total Lagrangian velocities to yield $\mathbf{u}'$. The problem was addressed because of the persistent west-southwestward mean migration motion of the rings responsible for the looping floats behavior, which produced zonal autocovariance functions persistently shifted towards positive values. The issue was not raised in VGRM for the data sampling was too low to give a statistically significant indication of such an effect.

Although in our particular case a splined mean flow computed from the non-loopers only did not change significantly the eddy statistics, it is suggested that mean flow estimates from Lagrangian data should be carried out by using the non-looping floats only because of the self-propelled nature of the loopers embedded inside the coherent vortices.

References

Alves, M. L. G. R. and A. Colin de Verdiere. 1999. Instability dynamics of a subtropical jet and applications to the Azores Front Current system: eddy-driven mean flow. J. Phys. Oceanogr., *29*, 837–864.

Bauer, S., M. S. Swenson and A. Griffa. 2002. Eddy-mean flow decomposition and eddy-diffusivity estimates in the tropical Pacific Ocean. 2. Results. J. Geophys. Res., *107*, 3154, doi:10.1029/2001JC000613.

Bauer, S., M. S. Swenson, A. Griffa, A. J. Mariano and K. Owens. 1998. Eddy-mean flow decomposition and eddy-diffusivity estimates in the tropical Pacific Ocean. 1. Methodology. J. Geophys. Res., *103*, 30855–30871.

Berloff, P. S. and J. C. McWilliams. 2002. Material transport in oceanic gyres. Part II: Hierarchy of stochastic models. J. Phys. Oceanogr., *32*, 797–830.

Berloff, P. S., J. C. McWilliams and A. Bracco. 2002. Material transport in oceanic gyres. Part I: Phenomenology. J. Phys. Oceanogr., *32*, 764–796.

Bleck, R., C. Rooth, D. Hu and L. T. Smith. 1992. Salinity-driven thermocline transients in a wind- and thermohaline-forced isopycnic coordinate model of the North Atlantic. J. Phys. Oceanogr., *22*, 1486–1505.

Bleck, R. and E. P. Chassignet. 1994. Simulating the ocean circulation with isopycnic-coordinate models, *in* The Oceans: Physical-Chemical Dynamics and Human Impact, S. K.Majumdar, ed.. The Pennsylvania Academy of Science, 17–39.

Bograd, S. J., R. E. Thomson, A. B. Rabinovich and P. H. LeBlond. 1999. Near-surface circulation of the northeast Pacific Ocean derived from WOCE-SVP satellite-tracked drifters. Deep-Sea Res. II, *46*, 2371–2403.

Borgas, M. S., T. K. Flesch and B. L. Sawford. 1997. Turbulent dispersion with broken reflectional symmetry. J. Fluid Mech., *279*, 69–99.

Bower, A. S., D. M. Fratantoni, W. E. Johns and H. Peters. 2002. Gulf of Aden eddies and their impact on Red Sea Water. Geophys. Res. Lett., *29*, 21, doi:10.1029/2002GL015342.

Bracco, A., J. H. LaCasce and A. Provenzale. 2000*a*. Velocity probability density functions for oceanic floats. J. Phys. Oceanogr., *30*, 461–474.

Bracco, A., J. H. LaCasce, C. Pasquero and A. Provenzale. 2000*b*. The velocity distribution of barotropic turbulence. Phys. Fluids, *12*, 2478–2488.

Brown, O. B., P. C. Cornillon, S. R. Emmerson and H. M. Carle. 1986. Warm core rings: a statistical study of their behavior. Deep-Sea Res., *33*, 1459–1473.

Brundage, W. L. and J. P. Dugan. 1986. Observations of an anticyclonic eddy of $18°$C water in the Sargasso Sea. J. Phys. Oceanogr., *16*, 717–727.

Bryden, H. L. and E. C. Brady. 1989. Eddy momentum and heat fluxes and their effects on the circulation of the Equatorial Pacific Ocean. J. Mar. Res., *47*, 55–79.

Chassignet, E. P., D. B. Olson and D. B. Boudra. 1990. Motion and evolution of oceanic rings in a numerical model and in observations. J. Geophys. Res., *95*, 22121–22140.

Chassignet, E. P. and Z. D. Garraffo. 2001. Viscosity parameterization and the Gulf Stream separation, *in* From stirring to mixing in a stratified ocean, P.Muller and D.Henderson, eds. Proceedings 'Aha Huliko'a Hawaiian Winter Workshop (U. of Hawaii, January 15-19, 2001), 37–41.

Chereskin, T. K., M. Y. Morris, P. P. Niiler, P. M. Kosro, R. L. Smith, S. R. Ramp, C. A. Collins and D. L. Musgrave. 2000. Spatial and temporal characteristics of the mesoscale circulation of the California Current from eddy-resolving moored and shipboard measurements. J. Geophys. Res., *105*, 1245–1269.

Davis, R. E.. 1991. Observing the general circulation with floats. Deep-Sea Res., *38*(Suppl.), 531–571.

Davis, R. E.. 1998. Preliminary results from directly measuring mid-depth circulation in the tropical and South Pacific. J. Geophys. Res., *103*, 24619–24639.

Elhmaidi, D., A. Provenzale and A. Babiano. 1993. Elementary topology of two-dimensional turbulence from a Lagrangian view-point and single particle dispersion. J. Fluid Mech., *257*, 533–558.

Falco, P., A. Griffa, P.-M. Poulain and E. Zambianchi. 2000. Transport properties in the Adriatic Sea as deduced from drifter data. J. Phys. Oceanogr., *30*, 2055–2071.

Figueroa, H. A. and D. B. Olson. 1989. Lagrangian statistics in the South Atlantic as derived from SOS and FGGE drifters. J. Mar. Res., *47*, 525–546.

Foltz, G. R., J. A. Carton and E. P. Chassignet. 2004. Tropical instability vortices in the Atlantic Ocean. J. Geophys. Res., *109*(C03029), doi:10.1029/2003JC001942.

Fratantoni, D. M.. 2001. North Atlantic surface circulation during the 1990's observed with satellite-tracked drifters. J. Geophys. Res., *106*, 22067–22093.

Freeland, H., P. Rhines and H. T. Rossby. 1975. Statistical observations of the trajectories of neutrally buoyant floats in the North Atlantic. J. Mar. Res., *33*, 383–404.

Garraffo, Z. D., A. Griffa, A. J. Mariano and E. P. Chassignet. 2001*a*. Lagrangian data in a high resolution numerical simulation of the North Atlantic. II: On the pseudo-Eulerian averaging of Lagrangian data. J. Mar. Syst., *29*, 177–200.

Garraffo, Z. D., A. J. Mariano, A. Griffa, C. Veneziani and E. P. Chassignet. 2001*b*. Lagrangian data in a high resolution numerical simulation of the North Atlantic. I: Comparison with *in-situ* drifter data. J. Mar. Syst., *29*, 157–176.

Garraffo, Z. D., W. E. Johns, E. P. Chassignet and G. J. Goni. 2003. North Brazil Current rings and transport of southern waters in a high resolution numerical simulation of the North Atlantic, *in* Interhemispheric water exchange in the Atlantic Ocean, Malanotte-Rizzoli and Goni, eds. Vol. 68. Elsevier Oceanographic Series, 375–409.

Griffa, A.. 1996. Applications of stochastic particle models to oceanographic problems, *in* Stochastic Modeling in Physical Oceanography, P. M.R. Adler and B.Rozovskii, eds. Birkhäuser Verlag, 114–140.

Hallberg, R.. 2000. Time integration of diapycnal diffusion and Richardson number- dependent mixing in isopycnal coordinate ocean models. Monthly Weather Rev., *128*, 1402–1419.

Holland, W. R. and P. B. Rhines. 1980. An example of eddy-induced ocean circulation. J. Phys. Oceanogr., *10*, 1010–1031.

Inoue, H.. 1986. A least-square smooth fitting for irregularly spaced data: finite-element approach using the cubic B-spline basis. Geophysics, *51*, 2051–2066.

Jayne, S. R. and J. Marotzke. 2002. The oceanic eddy heat transport. J. Phys. Oceanogr., *32*, 3328–3345.

Joyce, T. M.. 1984. Velocity and hydrographic structure of a Gulf Stream warm-core ring. J. Phys. Oceanogr., *14*, 936–947.

Krauss, W. and C. W. Boning. 1987. Lagrangian properties of the eddy fields in the northern Atlantic as deduced from satellite-tracked buoys. J. Mar. Res., *45*, 259–291.

LaCasce, J. H.. 2000. Floats and f/H. J. Mar. Res., *58*, 61–95.

LaCasce, J. H. and A. Bower. 2000. Relative dispersion in the subsurface North Atlantic. J. Mar. Res., *58*, 863–894.

LaCasce, J. H. and K. G. Speer. 1999. Lagrangian statistics in unforced barotropic flows. J. Mar. Res., *57*, 245–274.

Lavender, K. L., R. E. Davis and W. B. Owens. 2000. Mid-depth recirculation observed in the interior Labrador and Irminger seas by direct velocity measurements. Nature, *407*, 66–69.

Leach, H., S. J. Bowerman and M. E. McCulloch. 2002. Upper-ocean eddy transports of heat, potential vorticity, and volume in the northeastern North Atlantic – “Vivaldi 1991”. J. Phys. Oceanogr., *32*, 2926–2937.

Lee, T. N., W. E. Johns, R. J. Zantopp and E. R. Fillenbaum. 1996. Moored observations of western boundary current variability and thermohaline circulation at 26.5° N in the subtropical North Atlantic. J. Phys. Oceanogr., *26*, 962–983.

Marshall, J., E. Jones, R. Karsten and R. Wardle. 2002. Can eddies set ocean stratification?. J. Phys. Oceanogr., *32*, 26–38.

Maurizi, A., A. Griffa, P.-M. Poulain and F. Tampieri. 2004. Lagrangian turbulence in the Adriatic Sea as computed from drifter data: Effects of inhomogeneity and nonstationarity. J. Geophys. Res., *109*(C18), 4010, doi:10.1029/2003JC002119.

McWilliams, J. C.. 1984. The emergency of isolated coherent vortices in turbulent flow. J. Fluid Mech., *146*, 21–43.

Olson, D. B.. 1980. The physical oceanography of two rings observed by the cyclonic ring experiment. Part II: Dynamics. J. Phys. Oceanogr., *10*, 514–528.

Olson, D. B.. 1991. Rings in the ocean. Annu. Rev. Earth Planet. Sci., *19*, 283–311.

Owens, W. B.. 1991. A statistical description of the mean circulation and eddy variability in the northwestern Atlantic using SOFAR floats. Progr. Oceanogr., *28*, 257–303.

Paiva, A. M., J. T. Hargrove, E. P. Chassignet and R. Bleck. 1999. Turbulent behavior of a fine mesh ($1/12^\circ$) numerical simulation of the North Atlantic. J. Mar. Syst., *21*, 307–320.

Papadakis, M. P., E. P. Chassignet and R. W. Hallberg. 2003. Numerical simulations of the Mediterranean sea outflow: impact of the entrainment parameterization in an isopycnic coordinate ocean model. Ocean Model., *5*, 325–356.

Pasquero, C., A. Provenzale and A. Babiano. 2001. Parameterization of dispersion in two-dimensional turbulence. J. Fluid Mech., *439*, 279–303.

Phillips, H. E. and S. R. Rintoul. 2000. Eddy variability and energetics from direct current measurements in the Antarctic Circumpolar Current South of Australia. J. Phys. Oceanogr., *30*, 3050–3076.

Pickart, R. S., T. K. McKee, D. J. Torres and S. A. Harrington. 1999. Mean structure and interannual variability of the Slopewater System south of Newfoundland. J. Phys. Oceanogr., *29*, 2541–2558.

Poulain, P.-M.. 2001. Adriatic Sea surface circulation as derived from drifter data between 1990 and 1999. J. Mar. Syst., *29*, 3–32.

Poulain, P.-M. and P. P. Niiler. 1989. Statistical analysis of the surface circulation in the California Current System using satellite-tracked drifters. J. Phys. Oceanogr., *19*, 1588–1603.

Provenzale, A.. 1999. Transport by coherent barotropic vortices. Annu. Rev. Fluid Mech., *31*, 55–93.

Reynolds, A. M.. 2002*a*. Lagrangian stochastic modeling of anomalous diffusion in two-dimensional turbulence. Phys. Fluids, *14*, 1442–1449.

Reynolds, A. M.. 2002*b*. On Lagrangian stochastic modelling of material transport in oceanic gyres. Physica D, *172*, 124–138.

Reynolds, A. M.. 2003. Third-order Lagrangian stochastic modeling. Phys. Fluids, *15*, 2773–2777.

Richardson, P. L.. 1980. Anticyclonic eddies generated near the Corner Rise seamounts. J. Mar. Res., *38*, 673–686.

Richardson, P. L.. 1983. Gulf Stream rings, *in* Eddies in Marine Science, A. R.Robinson, ed.. Springer-Verlag, 19–45.

Richardson, P. L.. 1993. A census of eddies observed in North Atlantic SOFAR float data. Progr. Oceanogr., *31*, 1–50.

Riser, S. C. and H. T. Rossby. 1983. Quasi-Lagrangian structure and variability of the subtropical western North Atlantic circulation. J. Mar. Res., *41*, 127–162.

Roemmich, D. and J. Gilson. 2001. Eddy transport of heat and thermocline waters in the North Pacific: a key to interannual/decadal climate variability?. J. Phys. Oceanogr., *31*, 675–687.

Sawford, B. L.. 1999. Rotation of trajectories in Lagrangian stochastic models of turbulent dispersion. Bound.-Layer Meteor., *93*, 411–424.

Schmid, C., Z. Garraffo, E. Johns and S. L. Garzoli. 2003. Pathways and variability at intermediate depths in the tropical Atlantic, *in* Interhemispheric water exchange in the Atlantic Ocean, Malanotte-Rizzoli and Goni, eds. Vol. 68. Elsevier Oceanographic Series, 233–268.

Schott, F. A., R. Zantopp, L. Stramma, M. Dengler, J. Fischer and M. Wibaux. 2004. Circulation and deep-water export at the western exit of the Subpolar North Atlantic. J. Phys. Oceanogr., *34*, 817–843.

Shenoi, S. S. C., P. K. Saji and A. M. Almeida. 1999. Near-surface circulation and kinetic energy in the tropical Indian Ocean derived from Lagrangian drifters. J. Mar. Res., *57*, 885–907.

Straneo, F., R. S. Pickart and K. Lavender. 2003. Spreading of Labrador sea water: and advective-diffusive study based on Lagrangian data. Deep-Sea Res., *50*, 701–719.

Taylor, G. I.. 1921. Diffusion by continuous movements. Proc. Lond. Math. Soc., *20*, 196–212.

Thomson, D. J.. 1986. A random walk model of dispersion in turbulent flows and its application to dispersion in a valley. Quart. J. R. Met. Soc., *112*, 511–530.

Thomson, D. J.. 1987. Criteria for the selection of stochastic models of particle trajectories in turbulent flows. J. Fluid Mech., *180*, 529–556.

Vastano, A. C., J. E. Schmitz and D. E. Hagan. 1980. The physical oceanography of two rings observed by the cyclonic ring experiment. Part I: physical structure. J. Phys. Oceanogr., *10*, 493–513.

Veneziani, M., A. Griffa, A. M. Reynolds and A. J. Mariano. 2004. Oceanic turbulence and stochastic models from subsurface Lagrangian data for the Northwest Atlantic Ocean. J. Phys. Oceanogr., *34*, 1884–1906.

Weiss, J.. 1991. The dynamics of enstrophy transfer in two-dimensional hydrodynamics. Physica D, *48*, 273–294.

Zhang, H.-M., M. D. Prater and T. Rossby. 2001. Isopycnal Lagrangian statistics from the North Atlantic Current RAFOS floats observations. J. Geophys. Res., *106*, 13817–13836.

Table captions

Table 1. Estimates of the Lagrangian parameters characterizing the eddy field in region RINGS, obtained from the non-looping (no-loop) and the cyclonic (cycl) trajectory subsets (for details on the method of computation, see VGRM, Appendix B). The symbols stand for the velocity variance $\sigma^2_{u,v}$ and the decorrelation time scale $T_{Lu,v}$ (subscripts u, v are for either zonal or meridional estimates), the root-mean-square velocity V_{rms}, the spin Ω, the oscillation time scale T_w, and the average radius r, respectively.

Table 2. Mean Eulerian $\zeta/2$ computed by temporally averaging the instantaneous values for each ring, and mean Lagrangian Ω obtained by averaging both in time and over the whole looper ensemble (units are days^{-1}). Also shown are the total number of loopers and the number of particle transition events taking place between looper and non-looper regimes or vice versa, for the specific ring.

Figure captions

Figure 1. (a) Spaghetti-plot of the 700 m simulated trajectories during the first month of MICOM simulation; (b) Number of independent observation n^* per 1° square bin. The light grey shadowed area marks the 700 m bathymetry line.

Figure 2. (a) Annual mean velocity field obtained at 700 m by averaging the MICOM-predicted Eulerian velocities, temporally over the one-year simulation period and spatially over $1^\circ \times 1^\circ$ bins; (b) Eddy kinetic energy field computed by binning the Lagrangian fluctuation field over 1° square bins.

Figure 3. Snapshot of the 700 m (a) Eulerian velocity amplitude $|\mathbf{u_E}|$, (b) relative vorticity ζ obtained from the $\mathbf{u_E}$ field, and (c) Okubo-Weiss parameter Q.

Figure 4. Contours of the Gulf Stream recirculation region RINGS superimposed on (a) the 700 m annual mean flow, (b) the eddy kinetic energy field, and (c) a snapshot of the Eulerian velocity amplitude $|\mathbf{u_E}|$, together with a sample of looping trajectories embedded inside simulated Gulf Stream cold-core rings. Only the latest 60-day long tracks are shown.

Figure 5. Lagrangian velocity eddy statistics in region RINGS. Left panels: autocovariance function for the zonal (solid line) and meridional (dashed line) component, obtained from (a) the overall Lagrangian data, and separately from (b) the non-loopers and (c) the cyclonic loopers. Right panels: crosscovariance functions (R_{uv} and R_{vu}, plotted as solid and dashed lines, respectively), computed from (d) the overall trajectories, (e) the non-looping, and (c) the cyclonic floats. The dotted lines denote the 95% Confidence Limit.

Figure 6. Plot of Ω versus the eddy kinetic energy computed from single trajectories longer than 60 days in RINGS. Blue (red) dots are used to denote floats shorter (longer) than 100 days. The angular velocity error bars are also drawn. The two dashed lines $\Omega = \pm 0.1 \mathrm{days}^{-1}$ delimit the Ω-threshold between the looper and non-looper regimes.

Figure 7. Velocity autocovariance functions computed in VGRM from observed Lagrangian data in the recirculation regions RECW (left panels) and RECE (right panels), using the overall data set (panels a,d for RECW, RECE, respectively), the non-loopers (b,e), and the loopers (c,f). Refer to VGRM for region location.

Figure 8. Snapshot at simulation day 204 of the zonal (left panels) and meridional (right panels) vertical cross-sections of ring 04. The upper two panels show the vertical structure of the Eulerian MICOM velocity $\mathbf{u_E}$, superimposed on the isopycnal layers (thin solid lines). The lower two panels depicts the structure of the relative vorticity field ζ. The units for the vertical axis are m.

Figure 9. (a) Evolution of the instantaneous Eulerian $\zeta/2$ field inside the core of ring 04 (thick black line), the 60-day running average $\zeta/2$ (red line), and the 60-day running average Lagrangian spin Ω computed from a sample of 7 looping trajectories trapped inside ring 04 (thin black lines). The dashed line marks the 0.1-threshold separating the looper and non-looper regimes. (b) Part of a core-looper trajectory inside ring 04 (solid line), and of a temporary looper which behaves overall as a non-looping float (dashed line), superimposed on a snapshot of the 700 m relative vorticity field ζ. Arrows along the trajectory tracks mark 10-day time intervals.

Figure 10. Similar to Fig. 9a, but for ring 01.

Figure 11. Similar to Fig. 9, but for ring 05A-B. Panels (b) and (c) contain two parts of the same trajectory whose Ω decreases from $\approx 0.4\,\mathrm{days}^{-1}$ to non-looping values between day 240 and 315, and then increases back to looping regime levels between day 315 and 360 (see panel (a)). The part of the looper associated with ring 05A is depicted in (b), while the second transition event between the non-looper to looper regime associated with ring 05B is shown in (c).

Table 1:

	$\sigma^2_{u,v}\,(\mathrm{cm}^2\,\mathrm{s}^{-2})$	$V_{rms}\,(\mathrm{cm}\,\mathrm{s}^{-1})$	$T_{Lu,v}$ (days)	$\Omega\,(\mathrm{days}^{-1})$	T_w(days)	r(Km)
no-loop	47.0 ± 0.5	9.5 ± 0.1	12.0 ± 0.2	$O(0.01)$	$O(600)$	$O(800)$
	44.3 ± 1.4		14.0 ± 0.6			
cycl	132.7 ± 9.4	16.4 ± 0.4	15.0 ± 1.3	0.21 ± 0.01	29.9 ± 0.9	67.5 ± 3.7
	136.9 ± 4.7		15.0 ± 0.6			

Table 2:

RING #	$\zeta/2$	Ω	# loopers	# transitions
01	0.33 ± 0.06	0.30 ± 0.06	9	1
02A	0.28 ± 0.08	0.24 ± 0.04	5	0
02B	0.25 ± 0.07	0.24 ± 0.05	11	0
03	0.20 ± 0.11	0.23 ± 0.03	3	0
04	0.31 ± 0.08	0.31 ± 0.03	11	2
05A	0.34 ± 0.06	0.19 ± 0.12	16	8
05B	0.27 ± 0.03	0.17 ± 0.05	6	3

Figure 1:

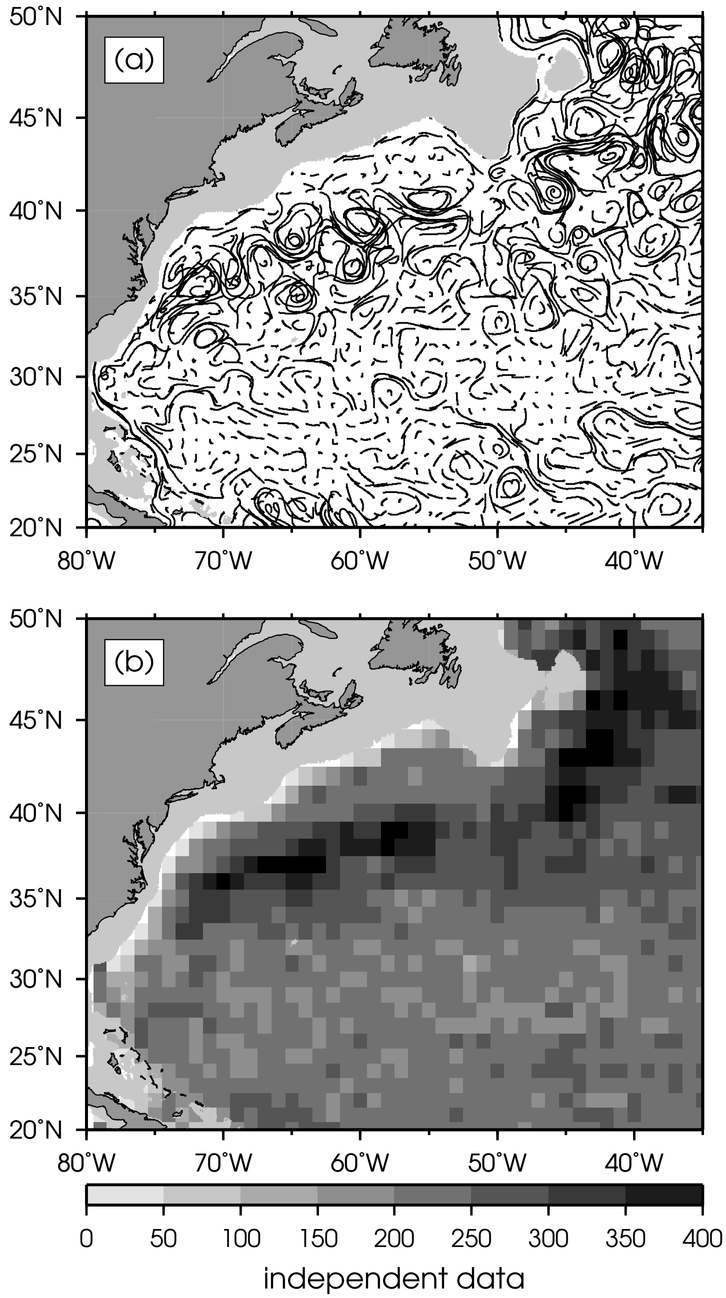

(a)
(b)
50°N
45°N
40°N
35°N
30°N
25°N
20°N
80°W
70°W
60°W
50°W
40°W
0
50
100
150
200
250
300
350
400
independent data

Figure 2:

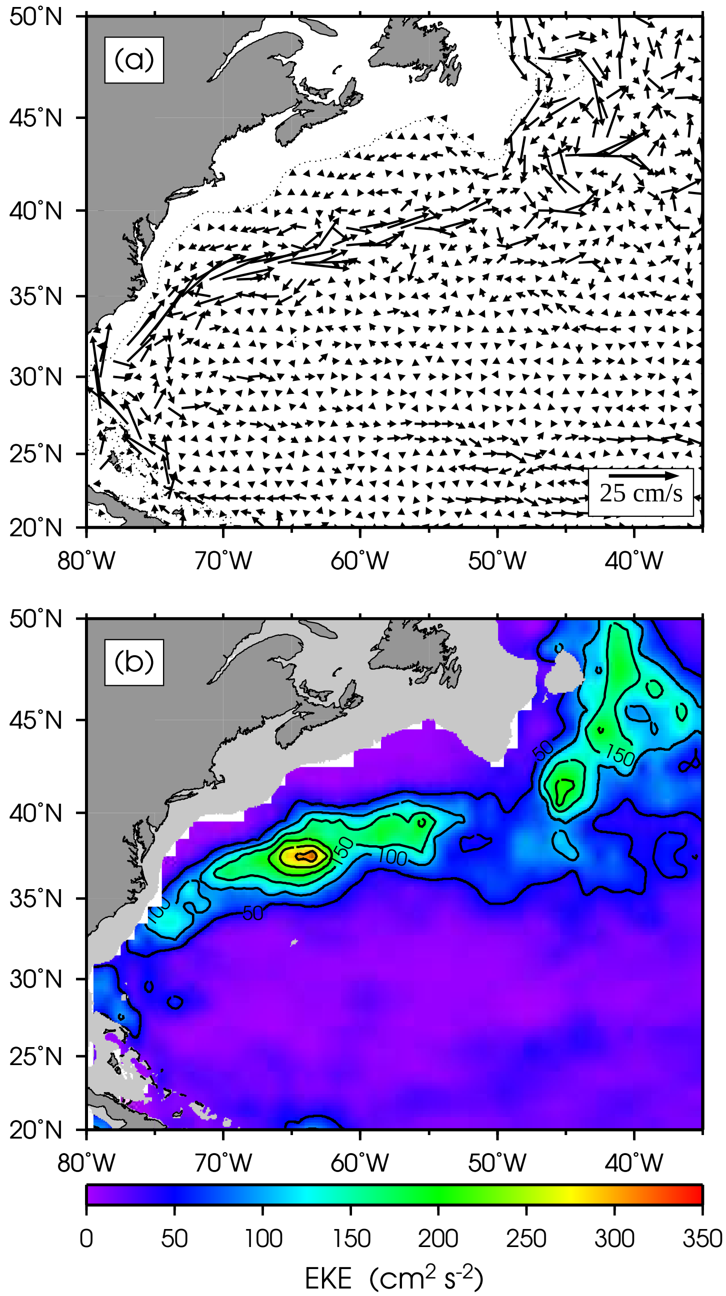
(a)
25 cm/s
50˚N
45˚N
40˚N
35˚N
30˚N
25˚N
20˚N
80˚W
70˚W
60˚W
50˚W
40˚W
(b)
50
100
150
EKE (cm^2 s^{-2})
0
50
100
150
200
250
300
350

Figure 3:

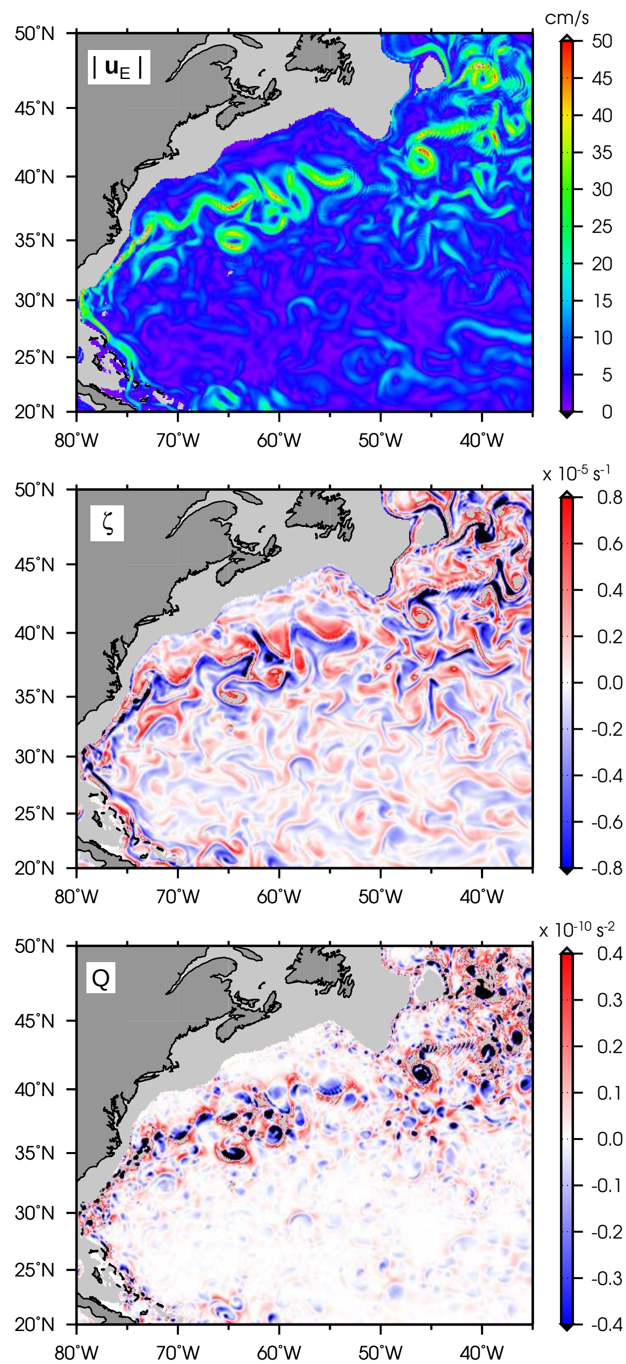
| uE |
cm/s
50
45
40
35
30
25
20
15
10
5
0
ζ
x 10-5 s-1
0.8
0.6
0.4
0.2
0.0
-0.2
-0.4
-0.6
-0.8
Q
x 10-10 s-2
0.4
0.3
0.2
0.1
0.0
-0.1
-0.2
-0.3
-0.4
50°N
45°N
40°N
35°N
30°N
25°N
20°N
80°W
70°W
60°W
50°W
40°W

Figure 4:

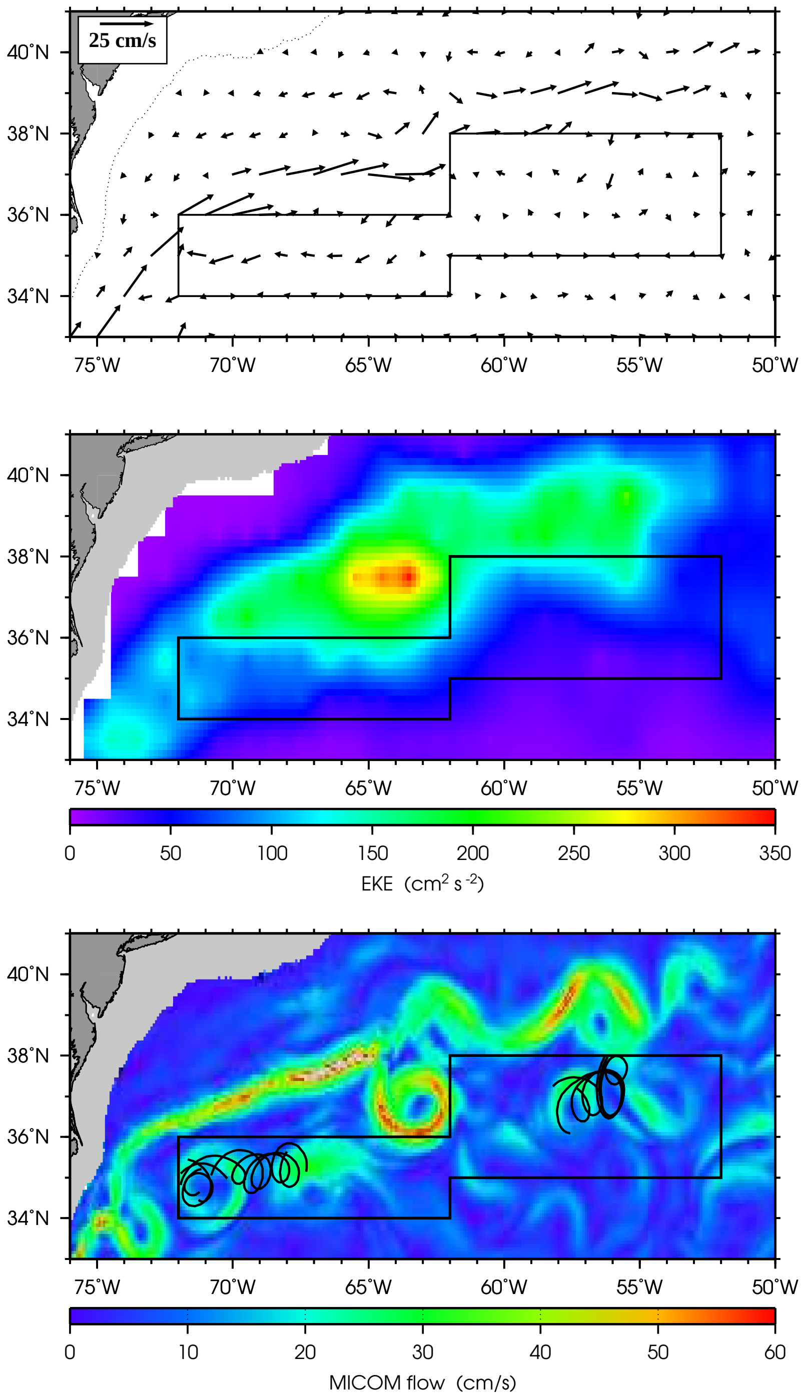
25 cm/s
40°N
38°N
36°N
34°N
75°W
70°W
65°W
60°W
55°W
50°W
0
50
100
150
200
250
300
350
EKE (cm² s⁻²)
0
10
20
30
40
50
60
MICOM flow (cm/s)

Figure 5:

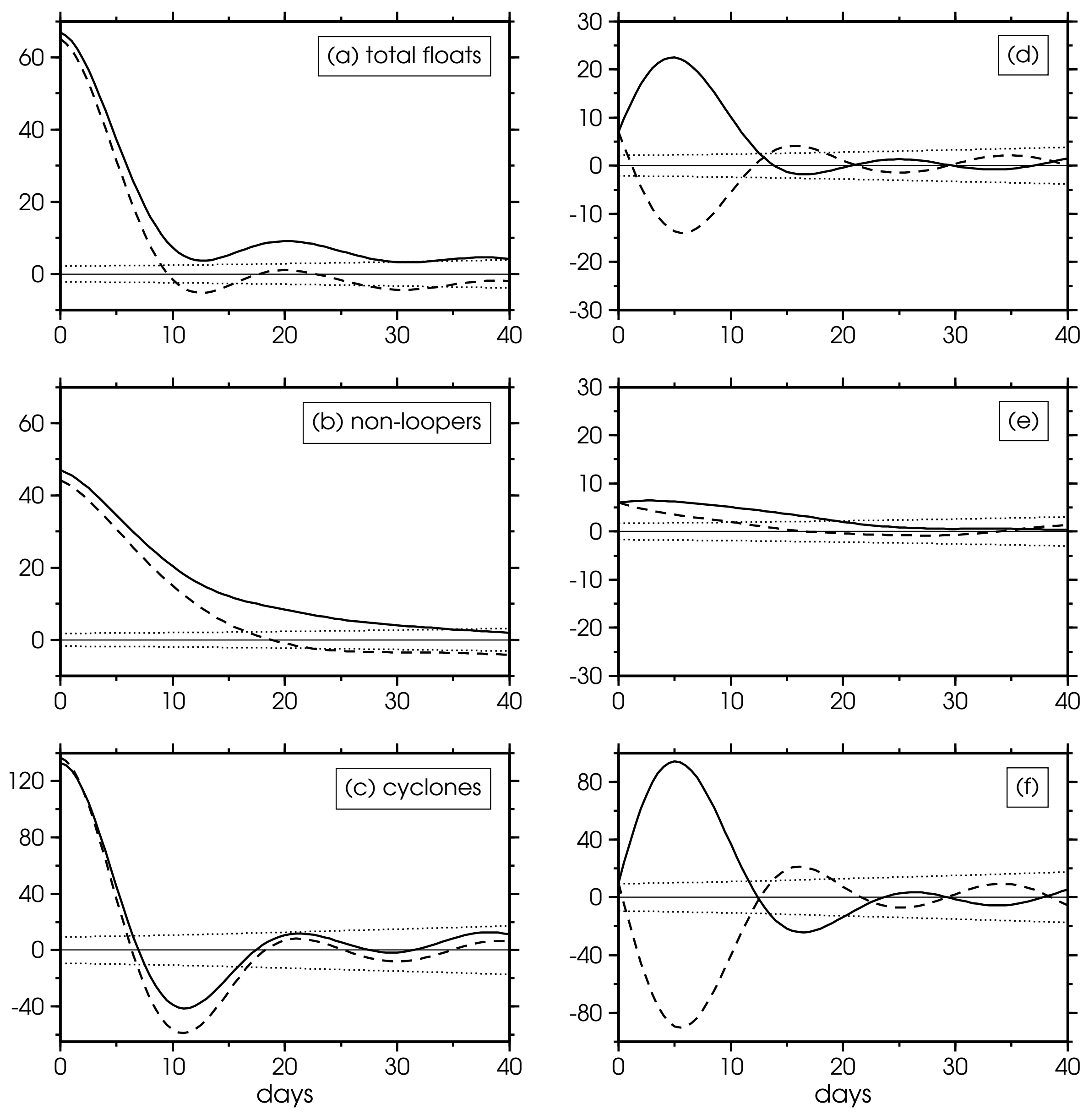

Figure 6:

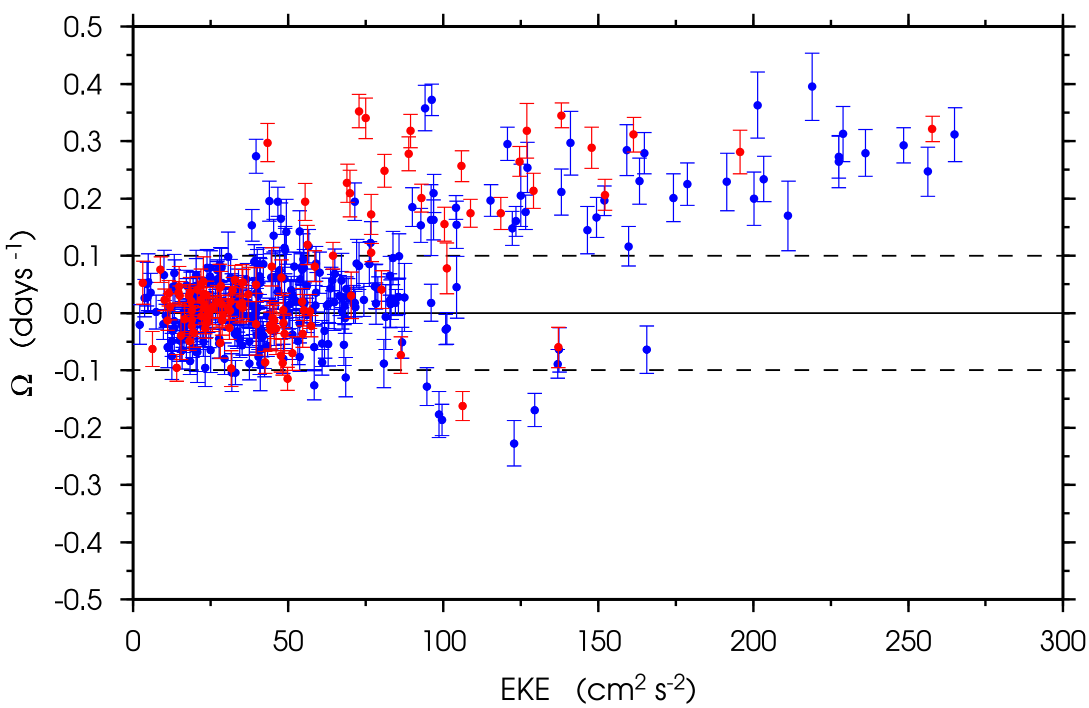

0.5
0.4
0.3
0.2
0.1
0.0
-0.1
-0.2
-0.3
-0.4
-0.5
Ω (days⁻¹)
0
50
100
150
200
250
300
EKE (cm² s⁻²)

Figure 7:

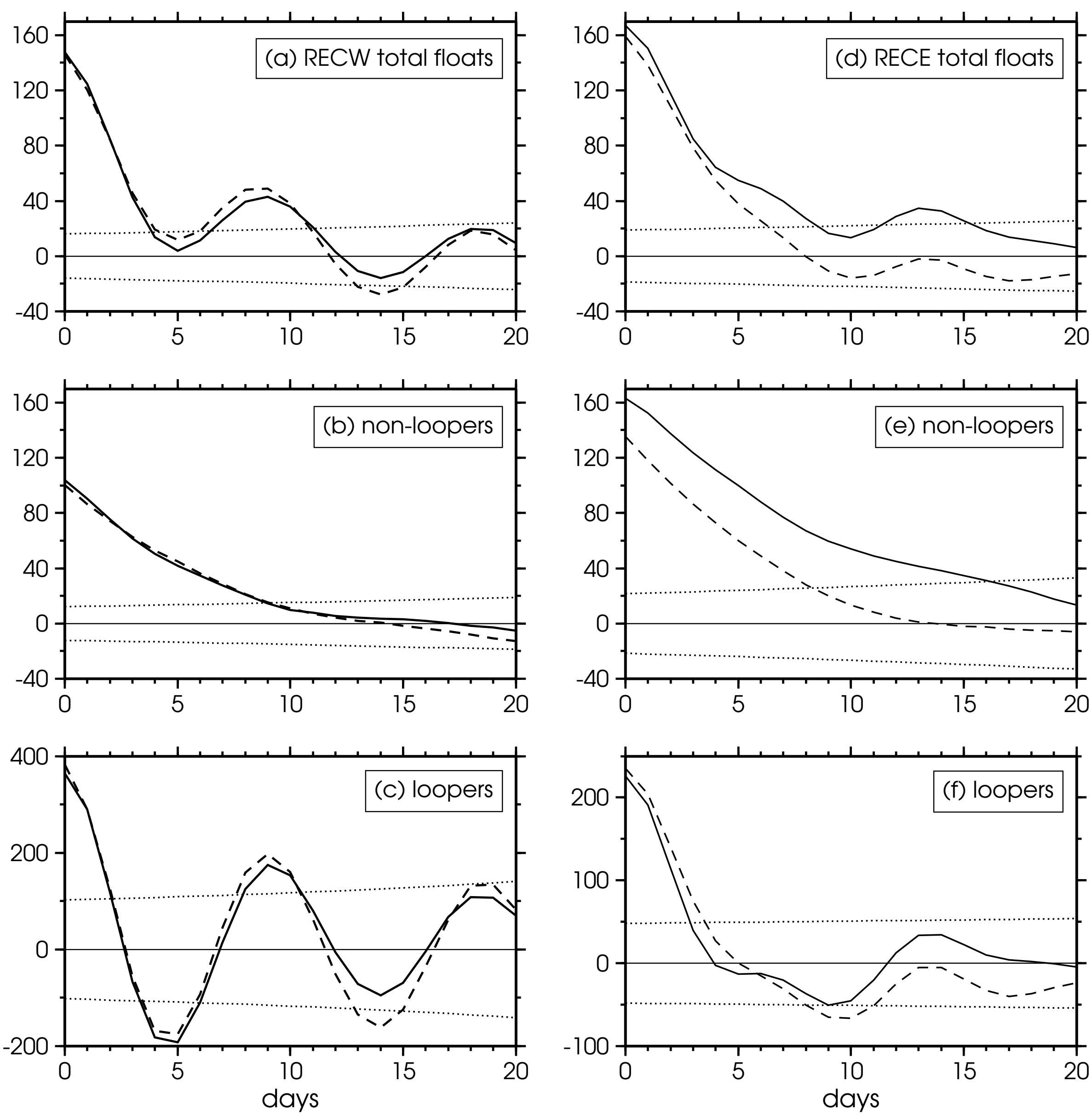
(a) RECW total floats
(b) non-loopers
(c) loopers
(d) RECE total floats
(e) non-loopers
(f) loopers
160
120
80
40
0
-40
400
200
0
-200
100
-100
0
5
10
15
20
days
days

Figure 8:

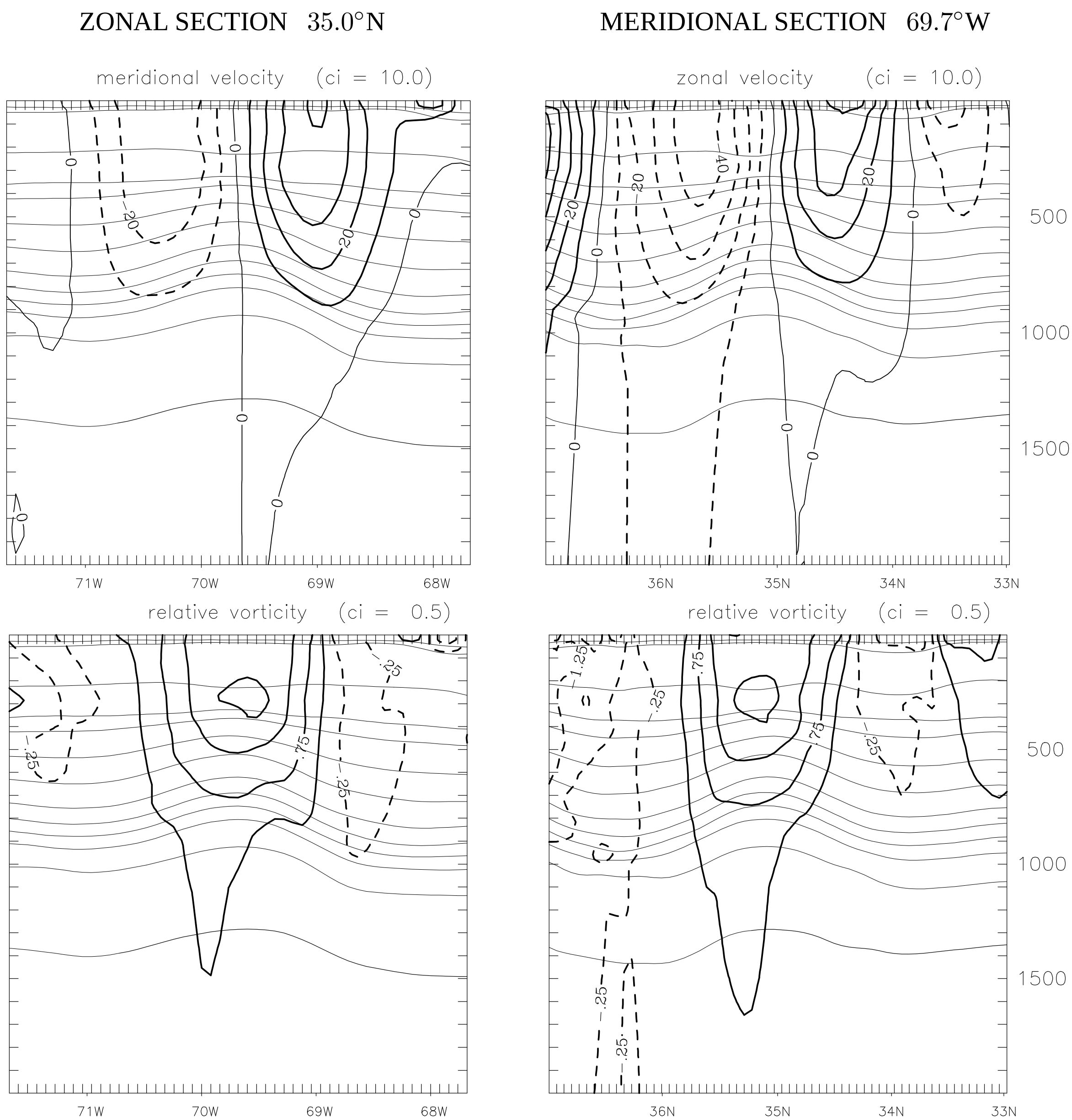

ZONAL SECTION 35.0°N
MERIDIONAL SECTION 69.7°W
meridional velocity (ci = 10.0)
zonal velocity (ci = 10.0)
relative vorticity (ci = 0.5)
relative vorticity (ci = 0.5)
71W
70W
69W
68W
36N
35N
34N
33N
500
1000
1500

Figure 9:

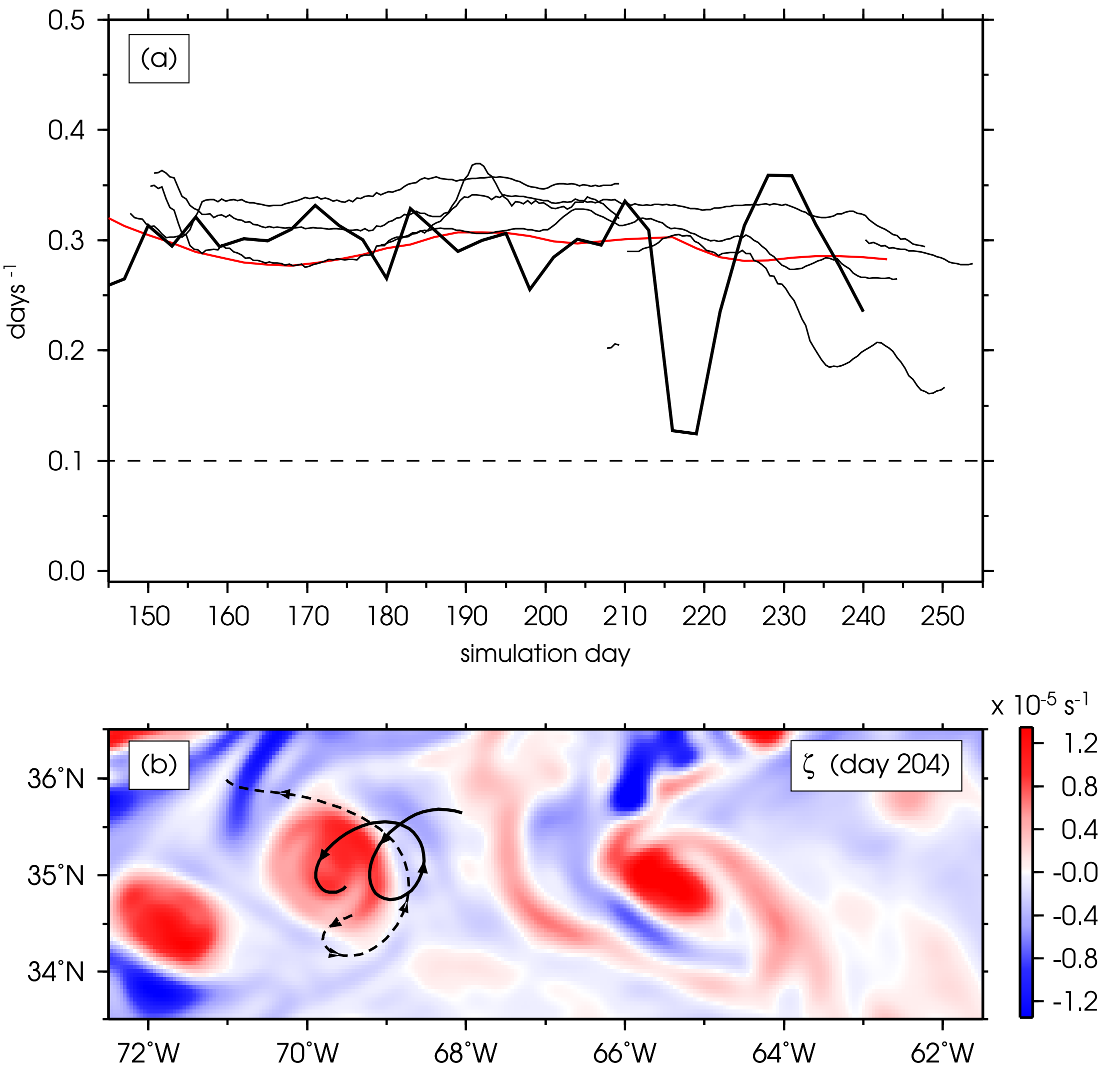

(a)
0.5
0.4
0.3
0.2
0.1
0.0
days -1
150
160
170
180
190
200
210
220
230
240
250
simulation day
(b)
ζ (day 204)
x 10-5 s-1
1.2
0.8
0.4
-0.0
-0.4
-0.8
-1.2
36˚N
35˚N
34˚N
72˚W
70˚W
68˚W
66˚W
64˚W
62˚W

Figure 10:

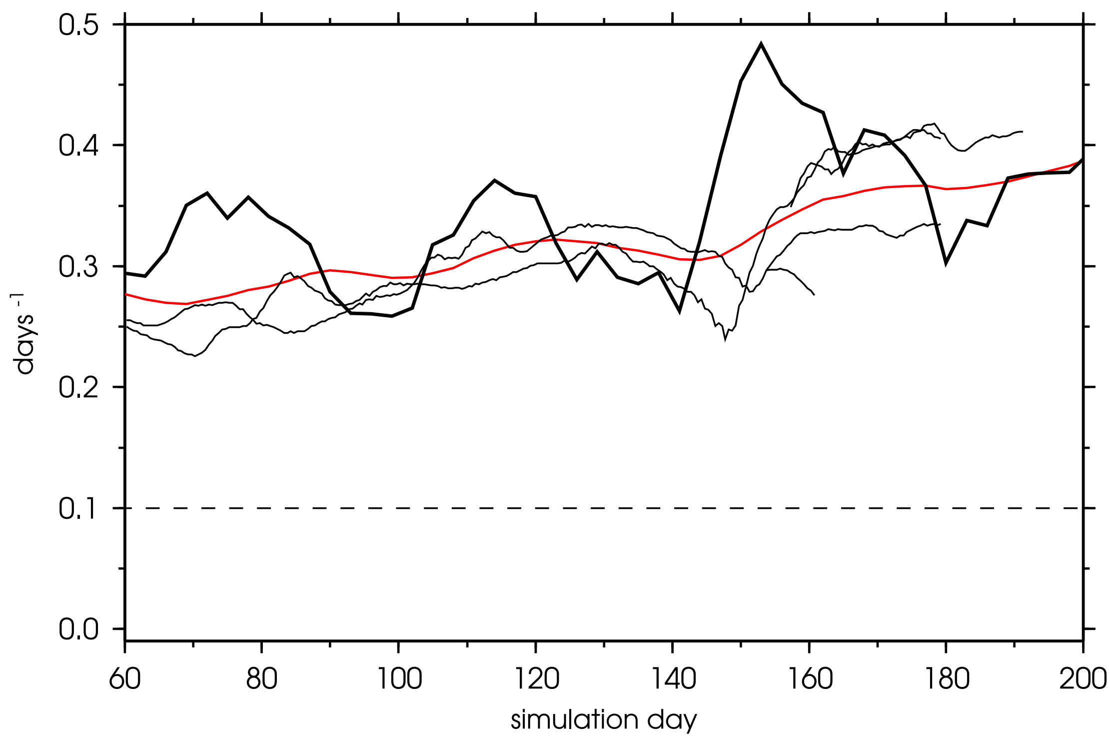

0.5
0.4
0.3
0.2
0.1
0.0
days $^{-1}$
60
80
100
120
140
160
180
200
simulation day

Figure 11:

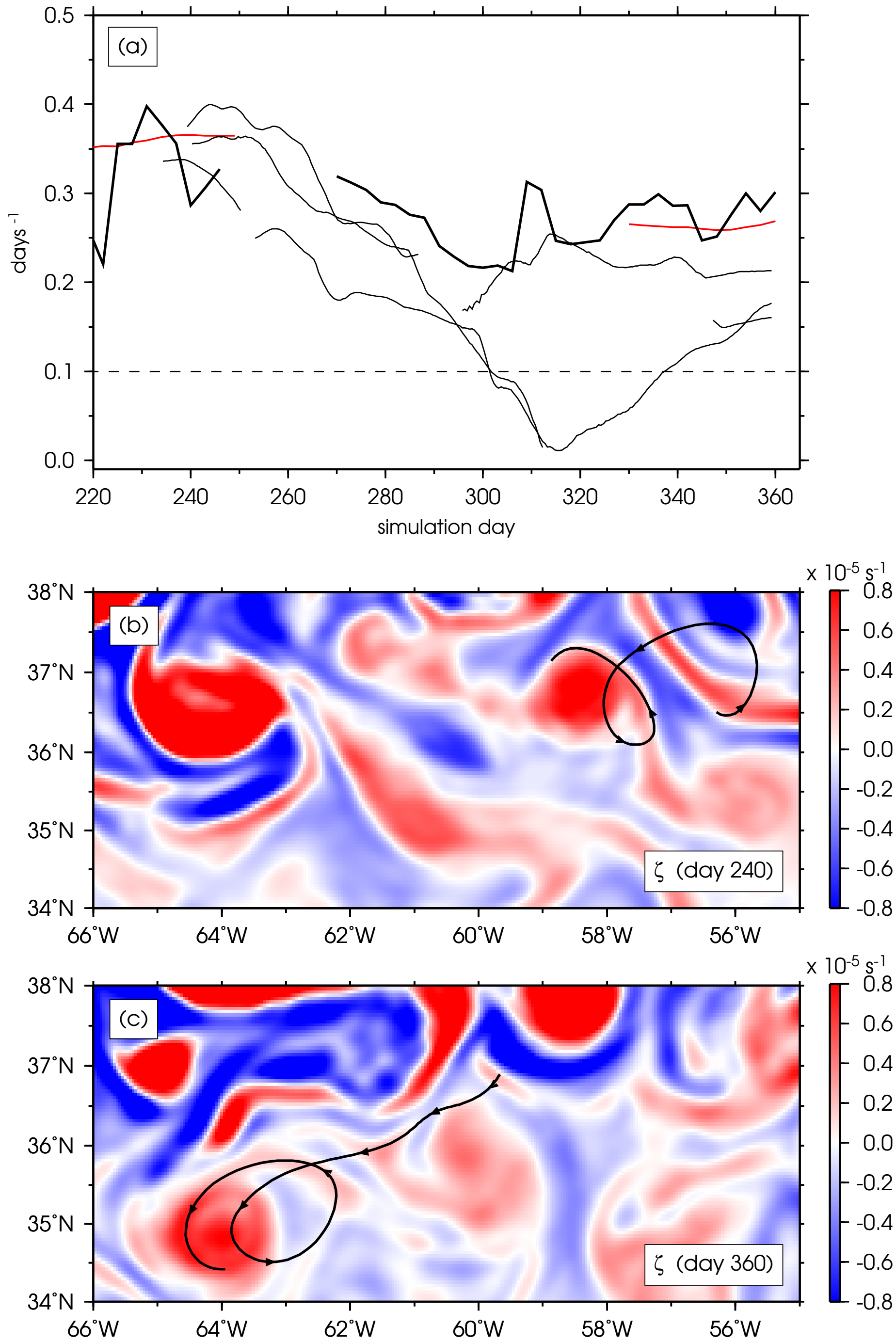

(a)
0.5
0.4
0.3
0.2
0.1
0.0
days -1
220
240
260
280
300
320
340
360
simulation day
(b)
38°N
37°N
36°N
35°N
34°N
66°W
64°W
62°W
60°W
58°W
56°W
x 10-5 s-1
0.8
0.6
0.4
0.2
0.0
-0.2
-0.4
-0.6
-0.8
ζ (day 240)
(c)
ζ (day 360)